Natural satellites astrometric data from either space probes and ground-based observatories produced by the European consortium "ESPaCE"

J.E. Arlot (1), N. Cooper (2), N. Emelyanov (3), V. Lainey (1), L.E. Meunier (1), C. Murray (2), J. Oberst (4), D. Pascu (5), A. Pasewaldt (4), V. Robert (1,6), R. Tajeddine (1,7), K. Willner (8)

(1): IMCCE, Institut de mécanique céleste et de vcalcul des éphémérides
(2) : QMUL, Queen Mary University of London
(3): SAI, Sternberg Astronomical Institute, Lomonosov University, Moscow
(4): DLR, Institute of Planetary Research, department of Planetary Geodesy
(5): U.S. Naval Observatory, Washington DC
(6): IPSA,Ecole d'ingénieurs aéronautique et spatiale
(7): Cornell University
(8): TUB, Technical University of Berlin

éditions

Institut de Mécanique Céleste *et de Calcul des Éphémérides*

Summary:

Introduction

The European FP7 ESPaCE program was appointed to provide ephemerides of the Natural planetary satellites in order to be used for the preparation of space missions. For the making of these ephemerides, astrometric observations were needed. Old data available were used but a new task was proposed: the making of the astrometric reduction of observations not yet reduced either ground-based observations (CCD or old photographic plates) and observations from space probes. For that purpose, a new software "CaViar" was elaborated. In the present publication, we present all the new astrometric observations reduced by the ESPaCE consortium.

1. Astrometric data from space probes

Introduction - Summary

This task concerns the reduction of astrometric images taken by the space probes Viking 1 and 2, Mariner 9, Voyager 1 and 2, Galileo and Cassini of the natural satellites of Mars, Jupiter and Saturn.

For that goal we adapted and used the CaVIaR software dedicated to the astrometric reduction of the images available on the Planetary Data Science (PDS) data base and understandable by the software SPICE used for the reduction. CaVIaR has been developed by Mike Evans from the Queen Mary University of London (QMUL) and improved in the framework of the present task. The objective is to re-reduce the data using recent reference star catalogues and to measure accurately the position of the centre of figure (COF) of the natural planetary satellites found on the images.

Contents of this section

I- Data from Viking 1 and 2
II- Data from Mariner 9
III- Data from Voyager 1 and 2
IV- Data from Galileo
V- Data from Cassini
VI- Data from Mars Express
VII- The Data base

1-I: Data from Viking 1 and 2

<u>Data</u>: Images of satellites of Mars, Phobos and Deimos.
It was not possible to have both a satellite and stars in the field so that the reduction was not simple to manage. Then, we decided to perform the measurement of the shift of the COF (Center of Figure) obtained from two models of the shape of Phobos: an ellipsoid and a 3D model (Digital terrain Model - DTM) provided by Konrad Willner of Technische Universität Berlin (TUB) based on the results of the reduction of TC Duxbury and JD Callahan. These measurements are completed.
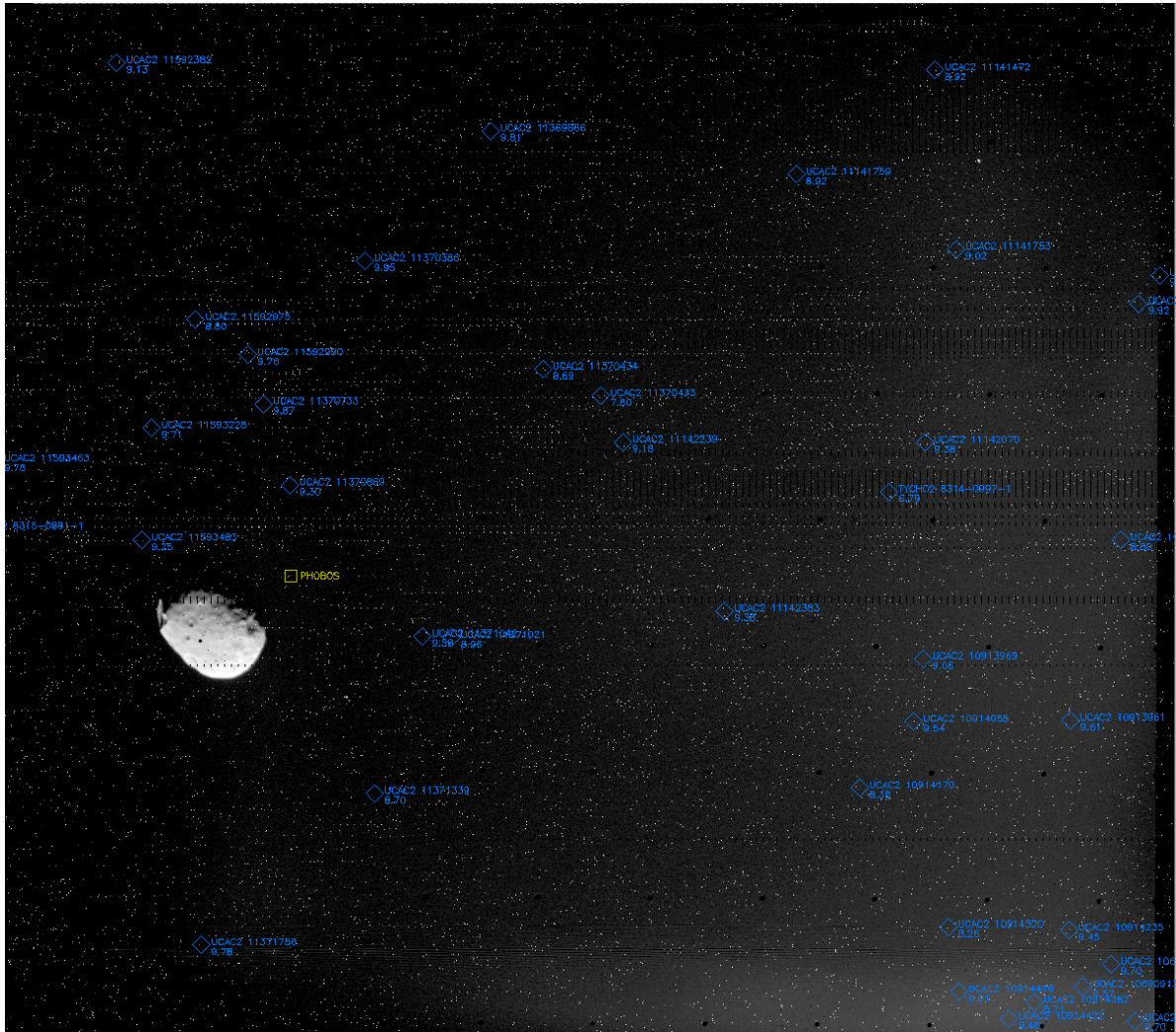
Image of Phobos from Viking 1 (f034a98)

The results are available directly through the NSDB Database (Arlot et al. 2016) where one will find the file *VO1_PHOBOS_results.txt* containing **103 reduced observations**, the file *VO2_PHOBOS_results.txt* containing **33 reduced observations**.

These two files are tabulated text with the description of the contents of each column on the first line of the files. In particular, there is the difference (in pixels, in kilometers on Phobos and in RA / Dec) between the position of the COF measured using the 3D model and that measured using an ellipsoid, and the uncertainty associated, except for data in RA / Dec.

The third file *Viking_models_offset_results.ods* is a table listing all the Viking images with their key information and notes about their treatment and the validity of results.

1-II: Data from Mariner 9

<u>Data</u>: Images of the satellites of Mars, Phobos and Deimos.
Since no information was provided about the pointing of the camera, it was not possible to perform an astrometric reduction.
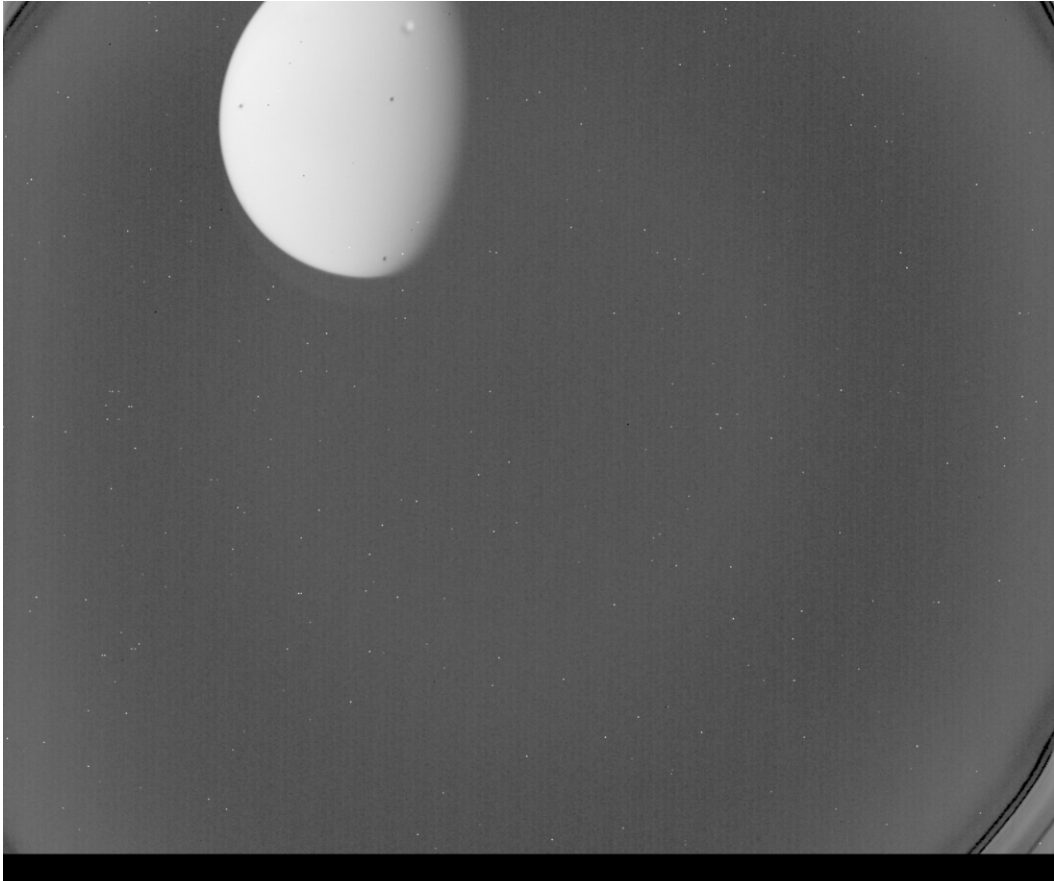
Image of Mars from the instrument ISS of Mariner 9 (01460397)

No SPICE kernels concerning the pointing of the camera (C-kernels) so that the one of the instrument (I-kernel) and the ones of the « Spacecraft » and of the « Planets » (SP-kernels) are available for the reduction of the data. More, stars are not detectable on the images of the satellites.

1-III: Data from Voyager 1 and 2

Data : Images of the satellites of Jupiter, Saturn, Uranus, Neptune: the headers of the images, in format « VICAR », are useless: the size of the images is not provided for extracting the images from the files. No reduction was possible for these images.

1-IV: Data from Galileo

Data : Images of the satellites of Jupiter
The images of the satellites do not allow to detect stars needed to calibrate the field of the camera.

1-V: Data from Cassini

<u>Data</u> : Images of the satellites of Jupiter and Saturn.
All the needed information for the calibration of the fields was available, so that the reduction was possible and the results are available on the NSDB data center (http://nsdb.imcce.fr)

1) Satellites of Jupiter

	Observations reduced / all	Quality of the images		
		good	saturated	Difficult to detect
Europe	34 / 301	6	5	23
Ganymede	29 / 342	2	13	14
Io	68 / 600	4	10	54

	Mean residuals : min/average/max (km)		Sigma min/average/max (km)
	in x	in y	in x and y
Europe	-75 / +45 / +105	-75 / +6 / +105	16 / 50 / 115
Ganymede	-150 / +55 / +150	-150 / +10 / +150	10 / 42 / 75
Io	-75 / -4.7 / +100	-75 / +15.5 / +100	7 / 123 / 200

<u>Comments:</u>

Among the large amount of available images, very few have been reduced. It was possible to distinguish the outlines of the satellite only on a small number of images while having enough stars to calibrate the field of the camera. On the other hand, some images show a satellite saturated with greater uncertainty about the actual position of the limb used to fit an ellipsoidal model; on other images it is difficult to distinguish the satellite itself from the background noise of the image. The necessary image treatment to get a measurable image was very hard to manage so that the uncertainty was larger after the image processing. Finally, only 12 images may be considered of good quality.
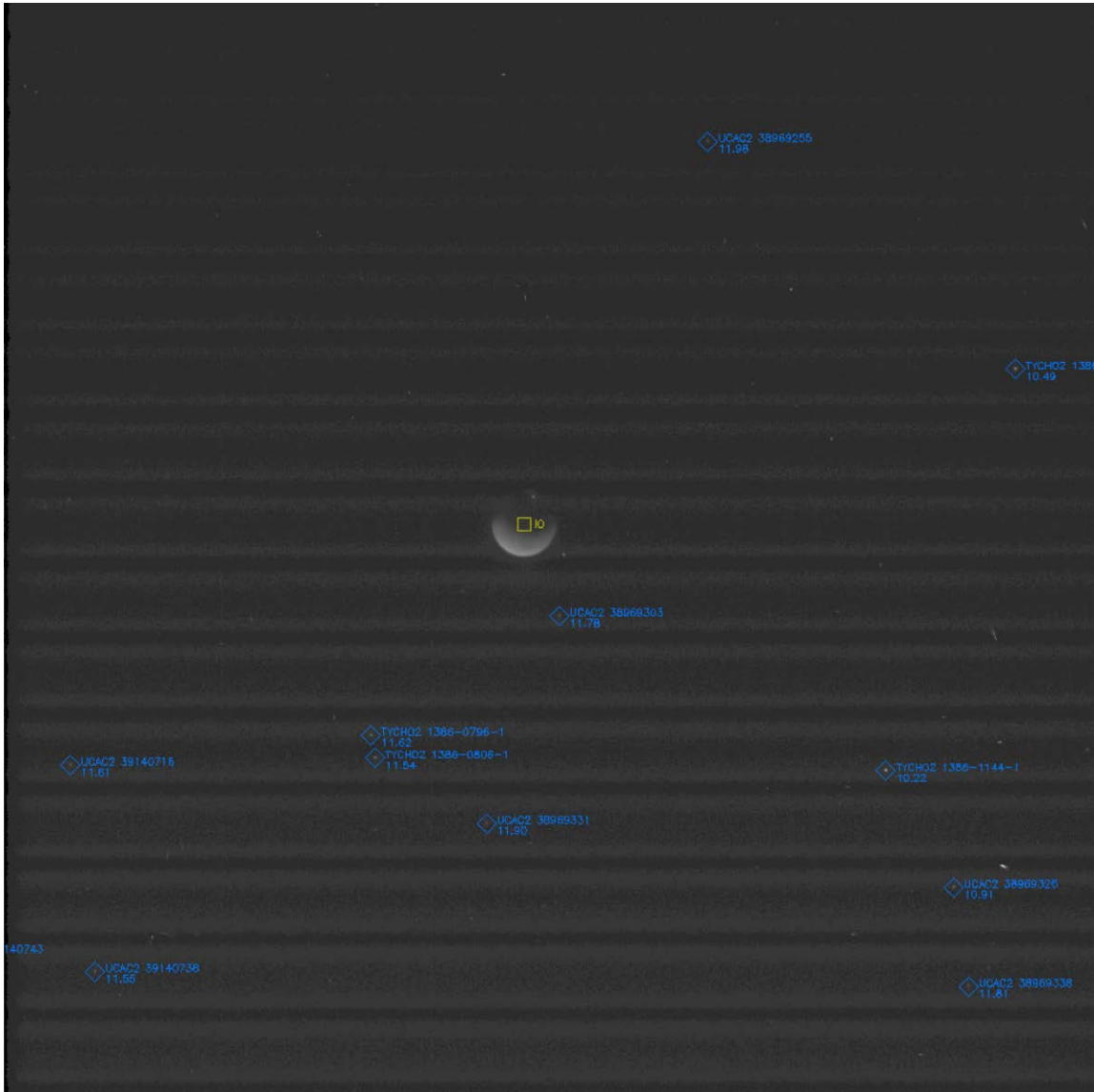
Image of Io from the instrument ISSNA of Cassini (N1356780329_1)

2) Satellites of Saturn

We encountered no problem with the astrometric reduction of the images of the satellites of Saturn. The results are as follows:

Sat:	Mimas	Enceladus	Tethys	Dione	Rhea	Iapetus
Nb obs.:	876	920	999	1361	1347	1533

Information is provided in Tajeddine, R.: UPMC PhD thesis, Paris, 2013.

Image from the Cassini space probe : Dione and Enceladus. . The field has been calibrated thanks to the faint stars visible on the image; Cassini Camera ISS, field 0°.35, Dione (1120 km) and Enceladus (512 km) Stars of mag 9 from UCAC2.

1-VI: Data from Mars Express
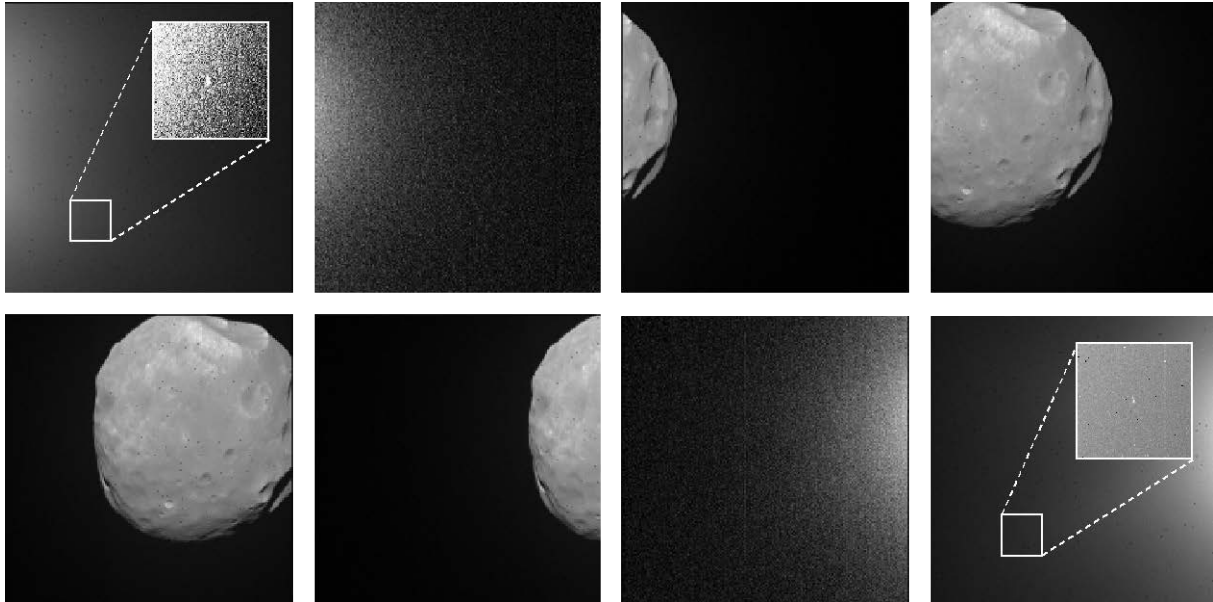
*Figure 1:Typical SRC image sequence observed during Phobos flyby in MEX orbit # 12917: First and last images are long-time exposures showing faint background stars (see magnified details). Exposure times in between are adjusted to the comparably bright Phobos disk. Black pixels on the surface of Phobos depict marked blemish pixels (an effect of degradation of the SRC CCD array (Oberst et al., 2008)). Before and after Phobos is crossing the SRC's field-of-view, the camera detects the bright Phobos shine.*

Data: Images of Phobos

The present data set includes 340 astrometric observations of Phobos with estimated uncertainties between 226 and 707 m (one-sigma). These observations have been derived from sequences of images taken with the Super Resolution Channel throughout 38 flybys performed by the Mars Express S/C between May 2013 and March 2014. The center of figure of the Martian moon was determined using the limb fit technique in combination with the latest 3-D shape model by Willner et al. (2014). Camera pointing was usually controlled at the beginning and end of each sequence by observing reference stars. Besides, images from orbits 12151, 12279, 12545, 12563, and 12598 offered the possibility of continuous pointing verification w.r.t. Jupiter and the Galilean moons, the Earth and Moon, or the Pleiades. Corrected and reduced observations are provided in right ascension and declination coordinates in the S/C-centered International Celestial Reference Frame (ICRF). To show the effect of fitting e.g. the MAR097 ephemeris to our observations the O-C (Observed minus Computed) residuals have been plotted in $RA \times \cos(Dec)$ and Dec.
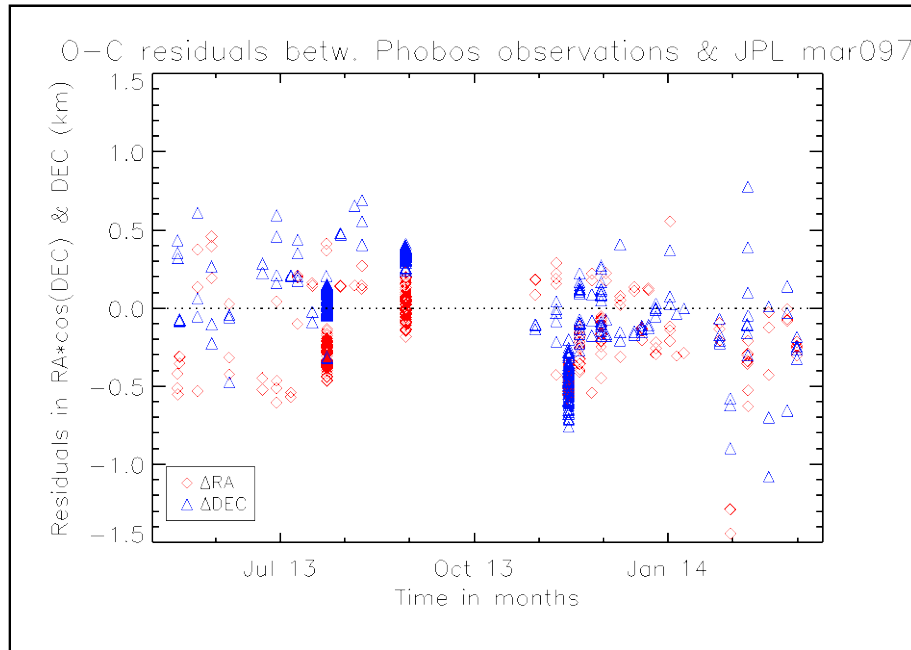
Figure 2: O-C offsets of our astrometric observations relative to the MAR097 orbit model: Variations between observations from different orbits are due to different accuracies in camera position and pointing. Variations between observations reduced from the same image sequence are assumed to be caused by S/C oscillations occurring as a consequence of attitude maneuvers.

The quality of our observations is estimated as sum of the uncertainties in S/C position, camera pointing, and COF measurement as described in detail in (Duxbury and Callahan, 1988; Willner et al., 2008; Pasewaldt et al., 2012). The following table depicts important parameters of the 38 MEX flybys of Phobos: the MEX orbit number, the mid-time of image sequence, the associated Phobos orbital position, distance to Phobos,and image resolution, the possibility for pointing verification.

MEX orbit number	Image-Seq. Time [UTC]	PhobosMA* [deg]	S/C-Phobos [km]	BGSD** [km]	Pointing Correction(Default: Star(s) in images # 1 & 8)
11908	2013-05-13T08:40	161.1	4074	0.037	
11911	2013-05-14T04:08	356.2	3534	0.032	
11940	2013-05-22T16:13	233.3	7929	0.072	
11963	2013-05-29T09:00	232.8	8392	0.076	
11992	2013-06-06T18:21	338.6	4266	0.039	
12046	2013-06-22T13:17	154.3	1355	0.012	
12069	2013-06-29T06:02	152.2	874	0.008	
12092	2013-07-05T22:48	151.0	346	0.003	Star(s) in images # 1 & 17
12103	2013-07-	175.4	4169	0.038	

	09T03:53				
12127	2013-07-16T03:36	140.2	1312	0.012	
12146	2013-07-21T16:23	265.6	16668	0.152	Phobos-Deimos
12150	2013-07-22T20:24	141.0	1028	0.009	
12151	2013-07-23T03:15	102.6	6528	0.059	Jupiter & Galilean satellites
12173	2013-07-29T13:08	137.6	1114	0.010	
12196	2013-08-05T05:56	138.0	1482	0.013	
12208	2013-08-08T17:58	129.3	2059	0.019	
12266	2013-08-25T15:42	125.1	2992	0.027	Mars background
12279	2013-08-29T11:04	101.1	6000	0.055	Pleiades
12301	2013-09-04T20:33	117.6	3610	0.033	Mars background
12348	2013-09-18T13:40	111.0	4404	0.040	Mars background
12383	2013-09-28T18:33	104.5	4540	0.041	w/o stars
12491	2013-10-30T00:18	75.9	5213	0.047	
12525	2013-11-08T21:46	81.2	3312	0.030	
12545	2013-11-14T18:36	225.5	12726	0.116	Earth & Moon
12563	2013-11-19T23:45	348.6	13901	0.127	Pleiades
12583	2013-11-25T19:22	71.0	2781	0.025	Star(s) in images # 1-3 &6-8
12598	2013-11-30T04:33	338.9	13624	0.124	Pleiades
12606	2013-12-02T12:06	68.9	2190	0.020	Star(s) in images # 1-4 &7-8
12629	2013-12-09T04:48	64.4	1840	0.017	
12652	2013-12-15T21:35	63.9	1206	0.011	
12664	2013-12-19T09:36	54.2	2543	0.023	
12675	2013-12-22T14:21	62.9	629	0.006	
12687	2013-12-26T02:26	55.9	1987	0.018	
12710	2014-01-01T19:10	53.8	1656	0.015	

12721	2014-01-04T23:54	60.8	560	0.005	
12733	2014-01-08T11:52	49.5	1514	0.014	
12791	2014-01-25T09:23	35.7	2780	0.025	
12808	2014-01-30T09:26	282.2	7166	0.065	
12836	2014-02-07T11:41	52.7	2774	0.025	
12837	2014-02-07T18:54	32.2	2790	0.026	
12871	2014-02-17T16:23	37.8	2458	0.022	
12901	2014-02-26T11:33	248.4	5440	0.050	
12917	2014-03-03T01:51	32.3	3069	0.028	
* MA – Mean Anomaly / ** BGSD – Best Ground Sampling Distance					

1-VII: The data base

The positions obtained after the reduction of the images were first put in the ftp espace repository as explained at the end of the present paper. They are also available through an easier access for the scientific community through the data base NSDB (nsdb.imcce.fr).

Conclusion

It appears a few months' delay in the processing of the different data. The first reason is the need to re-develop the CaVIaR program for use with a graphical interface as agreed between IMCCE (Institute of Celestial Mechanics and Ephemeris Computation) and QMUL (Queen Mary University of London), and facilitate the integration of new entries (new missions, new file format). The other reason is the difficulty to reduce the Viking data.and also the work made to analyze, understand and try to reduce the images from Mariner 9, Voyager 1 and 2 and Galileo that was finally not possible. Since it was possible to get astrometric data from Cassini, we added the reduction of Jupiter and Saturn system observations by Cassini in our framework. Numerous observations of high quality useful for ephemerides purpose are now available.

The list of the space probes images analyzed and the data extracted from these images are provided below; the list of data put in the NSDB data base is given at the end of the paper.

Table 1. Space probes data

Name of probes	Objects	Images number	References
VIKING	Martian satellites	137 images	NST IMCCE n°105, Paris
CASSINI	Jovian satellites	104 images	NST IMCCE n°105, Paris
CASSINI	Saturnian satellites	7032 images	A&A 2015 vol.575, A73 A&A 2013 vol.551, A129
.MARS EXPRESS	Martian satellites	370 images	NST IMCCE n°105, Paris

2. Astrometric data from digitized photographic plates

Plates of the Martian, Jovian and Saturnian systems from USNO were digitized and astrometric data were extracted after astrometric reduction. The data are available through the data base http:nsdb.imcce.fr.

2-I USNO Martian satellites images

The IMCCE analyzed the DAMIAN images of the USNO Martian photographic plates. Positions of the planet and its satellites are given. This chapter summarizes which conditions were encountered, which methods were used to provide the results and how to understand the result files.

2-I.1 - DAMIAN images and preliminary treatment

From 2011 December to 2012 April, the IMCCE received 427 DAMIAN images of the USNO Martian photographic plates from ROB. 150 photographic plates were taken with the USNO 61-inch refractor, 277 photographic plates were taken with the USNO 26-inch refractor. A very few duplicates and substitutions with Saturn images were found, the final number of available USNO Martian images is 420.

The IMCCE saw that some images were missing with regard to the list of USNO Martian plates that was transmitted by the ROB. IMCCE recently understood that the missing plates were not transmitted to ROB by Dan Pascu.

> I.1.1 - Negative to positive
> Since the negative fits format is not convenient to extract all the available informations, the IMCCE contacted the ROB to develop software to convert negative images to positive images. This was done and the software was provided to IMCCE. All the negative DAMIAN images were converted by IMCCE.

> I.1.2 - Direct and reverse (D-R) digitization effect
> The IMCCE asked the ROB to get D-R digitizations of each USNO photographic plate, in order to correct the object measured positions for an eventual digitization effect that should be estimated. All the DAMIAN images were provided in direct and reverse modes.

> I.1.3 - Machine stability
> The IMCCE wondered if we were sure of the stability of the scanning machine. It asked the ROB to get several and successive D-R digitizations of the available cluster plates, in order to estimate the short and long term stabilities of the DAMIAN machine with real data, to estimate an eventual D-R digitization effect and to calibrate the 26-inch parameters with a good accuracy (there are no cluster plates with the 61-inch). ROB explained that the machine stability was demonstrated, and that the available cluster plates were already digitized three years ago. With regard to these mentions, it was no need to the ROB to provide the several and successive D-R digitizations of the available cluster plates.

I.1.4 - Optical distortion
The use of an optical unit introduces field distortions in the images. The IMCCE asked the ROB to get several results of distortion tests (Moving Dot process). In fact, the Moving Dot process should be realized at least for each digitization session. The ROB considered that the machine stability was demonstrated and the distortion parameters did not change. So, the IMCCE uses the distortion profiles that were made three years ago. However, the ROB transmitted one distortion profile more. The DAMIAN optical distortion was corrected for each image by IMCCE with average data.

2-I.2 - Identification of the objects

A specific process was developed to extract, measure and identify the object positions on the images.

The stars were extracted and measured by means of the Source Extractor software, the planet and its satellites were extracted and measured by means of an adapted IDL program. The objects were then identified by comparing with corresponding catalogs and ephemerides. The method was initially developed with the analysis of the USNO Galilean plates.

In more details: the planet position is measured with an elliptical fitting, the satellite positions are measured once the background (the filter's halo) in the image central zone is substracted.
Tests were performed with different methods of measurement to produce valuable statistics and comparisons before defining the appropriate process: no correction of the background, Gaussian fitting, combination of a Gaussian and a quadratic fitting, Lorentzian fitting, barycenter measurement… The IMCCE considered that the ellipse fitting method provided the best results, by comparing the measured positions with the most recent ephemerides. But we should note that the satellite position may not be extracted with a sufficient accuracy when its distance to the planet was below 0.7' typically which corresponds to 107 images among 420.

2-I.3 - Astrometric reduction

Because of the few available stars, the astrometric reduction is quite different with a common one.

I.3.1 - UCAC2 star spherical coordinates
The star catalog coordinates were directly corrected for all-known spherical effects such as the proper motions, the parallaxes, the light aberration, the relativistic light deflexion of the Sun and Mars, and the total atmospheric refraction.

I.3.2 - UCAC2 star measured coordinates
The star measured coordinates were corrected for the instrumental coma-magnitude effect (determined three years ago thanks to the cluster plates analysis) when the 26inch was used. No instrumental corrections were applied when the 61inch was used because there are no cluster plates available in this case.

I.3.3 - Calibration of the field
When UCAC2 stars were available, the field was calibrated with a 4-parameters model that takes into account the temperature variation in the case of the 26-inch observations, and by a 6-parameters model in the case of the 61inch observations, in order to provide (RA,Dec) positions. When no stars could be used for the calibration, the field was calibrated with a 4-parameters model with mean offsets, scale and orientation plate constants, in order to provide relative positions to the planet.

I.3.4 - Measured positions
The measured planet and satellite positions were corrected for the phase effect and for the above reverse effects to provide positions in a geocentric ICRS frame, outside the atmosphere. In consequence, no spherical corrections should be applied to use the data.


2-I.4 - Position results

There are different kinds of available astrometric results:

- Spherical (RA,Dec) positions of the planet and its satellites are available in a geocentric ICRS frame, in degrees, when the astrometric reduction with UCAC2 stars provided a sufficient accuracy. There are 529 positions of Mars, 317 positions of Phobos and 401 positions of Deimos. The mean positioning accuracy (rms residuals) is 62 mas for the planet, 68 mas for Phobos and 62 mas for Deimos. These positioning results are used to produce intersatellite and relative (RA,Dec) statistics.
214 intersatellite positions of Deimos relative to Phobos provide a mean positioning accuracy (rms residuals) of 43 mas. 285 relative (RA,Dec) positions of Phobos to the planet provide a mean positioning accuracy (rms residuals) of 50 mas. 355 relative (RA,Dec) positions of Deimos to the planet provide a mean positioning accuracy (rms residuals) of 51 mas.

- Relative (X,Y) tangential positions of Phobos and Deimos to the planet were calculated with a mean astrometric reduction process (4-parameters model with mean offsets, scale and orientation plate constants) when no stars were available for the field calibration. Relative tangential positions of Phobos and Deimos are available in a geocentric ICRS frame, in arcsec. There are 102 relative positions of Phobos and 99 relative positions of Deimos. The mean positioning accuracy (rms residuals) is 87 mas for Phobos and 85 mas for Deimos.

- Spherical (RA,Dec) positions of the planet were deduced from spherical (RA,Dec) positions of the satellites and are available in a geocentric ICRS frame, in degrees. There are 318 positions of the planet deduced from Phobos spherical coordinates and 402 positions of the planet deduced from Deimos spherical coordinates. The mean positioning accuracy (rms residuals) is 60 mas for positions deduced from Phobos and 52 mas for positions deduced from Deimos.

The mean position accuracies detailed above were calculated by comparing the measured positions of the planet and its satellites with the INPOP10 planetary ephemeride (Fienga et al., 2010) and the last IMCCE satellite model (Lainey et al., 2007).
The figures below show the spherical (O-C) distributions in right ascension and declination as functions of the date of observation.
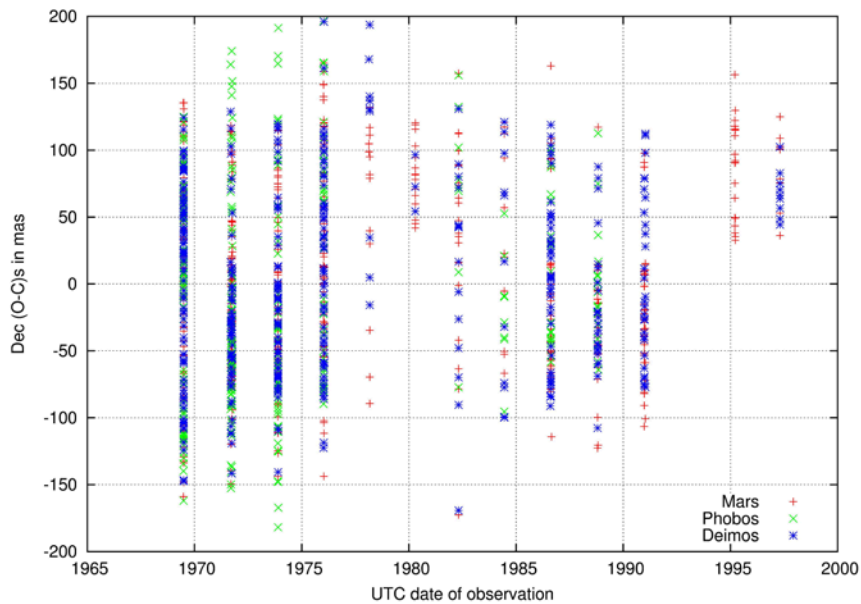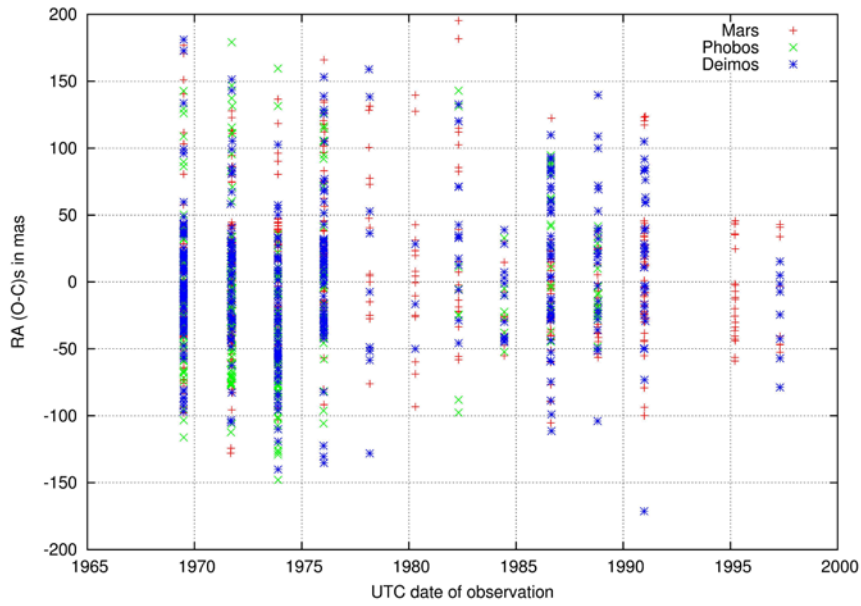
These results are very encouraging and we demonstrate the high interest to continue the analysis of old photographic plates such as USNO's. The interest of these results in the frame of the ESPaCE project is also demonstrated. In fact:

- the spherical (RA,Dec) accuracy is about of 65 mas or 32 km,

- the intersatellite accuracy is about of 43 mas or 13 km, that is the same order of the positioning accuracy provided by the spacecrafts at this epoch,

a previous manual analysis of the USNO Martian plates (unpublished observations) provided 217 relative tangential positions of Phobos and 223 relative positions of Deimos (Lainey et al., 2007); the positioning accuracy was about of 200 mas or 60 km so the new positioning accuracy is 4 times better.

Results files containing the calculated positions and various statistics are available in tar archives:

1. the archive "USNO_Mars_RA_Dec_positions" contains result files with (RA,Dec) spherical positions of the planet and its satellites, in degrees, and corresponding statistics;
2. the archive "USNO_Mars_intersatellite_positions" contains result files with intersatellite (RA,Dec) spherical positions of Phobos relative to Deimos and deduced from the first (RA,Dec) positions, in degrees, and intersatellite statistics;
3. the archive "USNO_Mars_relative1_positions" contains result files with (RA,Dec) spherical positions of the satellites relative to the planet and deduced from the first (RA,Dec) positions, in degrees, and relative statistics;
4. the archive "USNO_Mars_relative2_positions" contains result files with tangential (X,Y) positions of the satellites relative to the planet, in arcsec, and corresponding statistics;
5. the archive "USNO_Mars_planet_positions" contains result files with (RA,Dec) spherical positions of the planet deduced from the satellite spherical coordinates, and corresponding statistics.

Each archive contains several files that correspond to the comparisons of the calculated positions with different satellite and Mars ephemerides. IMCCE (Lainey et al., 2007) and JPL (mar097) satellite ephemerides were compared. IMCCE (Fienga et al., 2008, 2009, 2010) and JPL (JPL memorandum, 2008, 2010) Mars ephemerides were compared: INPOP06, INPOP08, INPOP10, DE421 and DE423.

Files named "results_40*.txt" contain:

1. number
2. USNO plate and exposure identification
3. number of UCAC2 stars used in the astrometric reduction
4. DJJTB date
5. UTC date
6. RA position of the body in degrees (or arcsec for tangential results)
7. Dec position of the body in degrees (or arcsec for tangential results)
8. RA.cos(Dec) individual (O-C) in mas
9. Dec individual (O-C) in mas

A single file named "results_*.txt" gathers the data for the planet and its satellites.

Finally, each archive also contains several files that correspond to the global statistics of the comparisons of the calculated positions with the different satellite and Mars ephemerides.

Files named "results_*_stat_*.txt" contain:

1. the mean value of the individual RA.cos(Dec) (O-C)s
2. the mean value of the individual Dec (O-C)s
3. the rms residuals of the individual RA.cos(Dec) (O-C)s
4. the rms residuals of the individual Dec (O-C)s

This in the following order: Mars, Phobos and Deimos.

2-I.5 - Discussion

The results above were presented at the 44th DPS meeting of the American Astronomical Society in Reno in October, 2012, and to Dan Pascu and Norbert Zacharias in Washington in May, 2013.

It was there decided to redo the job by modifying the reference star catalog in order to get more source informations. By using the last available UCAC4 star catalog, it may be possible to get such data with more references. This in particular to correct the star positions for the last spherical effect due to the color of the objects. In fact and thanks to the preliminary work that was done with the analysis of the USNO Galilean plates, it was found a systematic and interesting effect that shifts the position objects in declination. We there found a similar effect that is less important in terms of magnitude, and because the color effect may introduce such a bias, it was decided to take it into account.

This modification explains the delay we have because we started to redo the job at the beginning of June, 2013. Now it is close to be finished: the entire Mars image collection will be ready for the final analysis at the end of January, 2014. The corresponding statistics will be available at the same time.

2-II - USNO Saturnian satellites images

The IMCCE analyzed parts of the DAMIAN images of the USNO Saturnian photographic plates. First positions of the satellites are given. This chapter summarizes which conditions were encountered and which methods were used to provide the results.

2-II.1 - DAMIAN images and preliminary treatment

From 2012 June to 2013 August, the IMCCE received 95 DAMIAN images of the USNO Saturnian photographic plates from ROB. These plates were taken with the USNO 61-inch refractor and with the USNO 26-inch refractor. A very few duplicates and substitutions were found, the final number of provided single images is 82. The IMCCE will also use the Saturnian digitizations that it made three years ago as mentioned in the D5.2 report.

II.1.1 Negative to positive
Since the negative fits format is not convenient to extract all the available informations, the IMCCE converted the 95 negative DAMIAN images provided by the ROB.

II.1.2 - Direct and reverse (D-R) digitization effect
The 95 DAMIAN images were provided in direct and reverse modes by the ROB.

II.1.3 - Optical distortion
The DAMIAN optical distortion was corrected for each image by IMCCE with average data as mentioned in section I.1.4.

2-II.2 - Identification of the objects

A specific process was developed to extract, measure and identify the object positions on the images.
The stars were extracted and measured by means of the Source Extractor software, the satellites were extracted and measured by means of an adapted IDL program. The objects were then identified by comparing with corresponding catalogs and ephemerides. The method was initially developed with the analysis of the USNO Martian plates.

In more details: the planet position is determined with an elliptical fitting using the Peng method (by converting the fits planet region to binary region), the satellite positions are measured once the background (the rings' halo) in the image central zone is substracted. The figure below shows of the rings could be substracted to allow the extraction of the closest satellites.

2-II.3 - Astrometric reduction

Because of the few available stars, the astrometric reduction is quite different with a common one.

II.3.1 - UCAC2 star spherical coordinates

The star catalog coordinates were directly corrected for all-known spherical effects such as the proper motions, the parallaxes, the light aberration, the relativistic light deflexion of the Sun and Saturn, and the total atmospheric refraction.

II.3.2 - UCAC2 star measured coordinates

The star measured coordinates were corrected for the instrumental coma-magnitude effect (determined three years ago thanks to the cluster plates analysis) when the 26inch was used. No instrumental corrections were applied when the 61inch was used because there are no cluster plates available in this case.

II.3.3 - Calibration of the field

When UCAC2 stars were available, the field was calibrated with a 4-parameters model that takes into account the temperature variation in the case of the 26-inch observations, and by a 6-parameters model in the case of the 61inch observations, in order to provide (RA,Dec) positions. When no stars could be used for the calibration, the field was calibrated with a 4-parameters model with mean offsets, scale and orientation plate constants, in order to provide relative positions to the planet.

II.3.4 - Measured positions

The measured satellite positions were corrected for the phase effect and for the above reverse effects to provide positions in a geocentric ICRS frame, outside the atmosphere. In consequence, no spherical corrections should be applied to use the data.

2-II.4 - Position results and discussion

Tens of images were first reduced before it was decided to redo the Martian's by modifying the reference star catalog. That's why the UCAC2 catalog is still there used. The figures below show the spherical (O-C) distributions in right ascension and declination as functions of the date of observation.
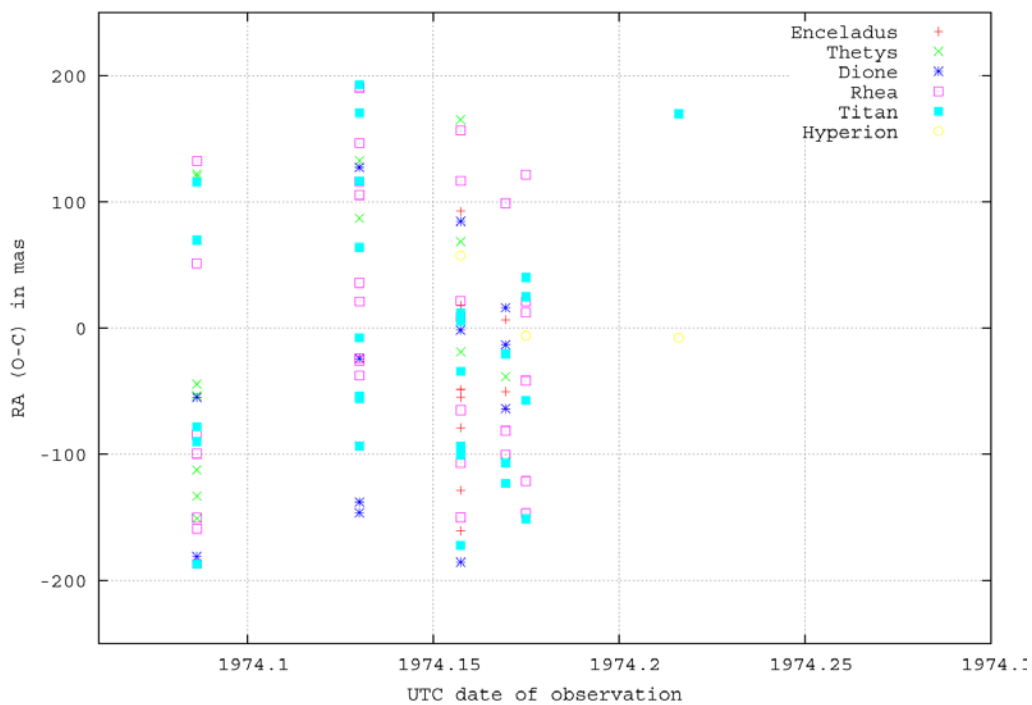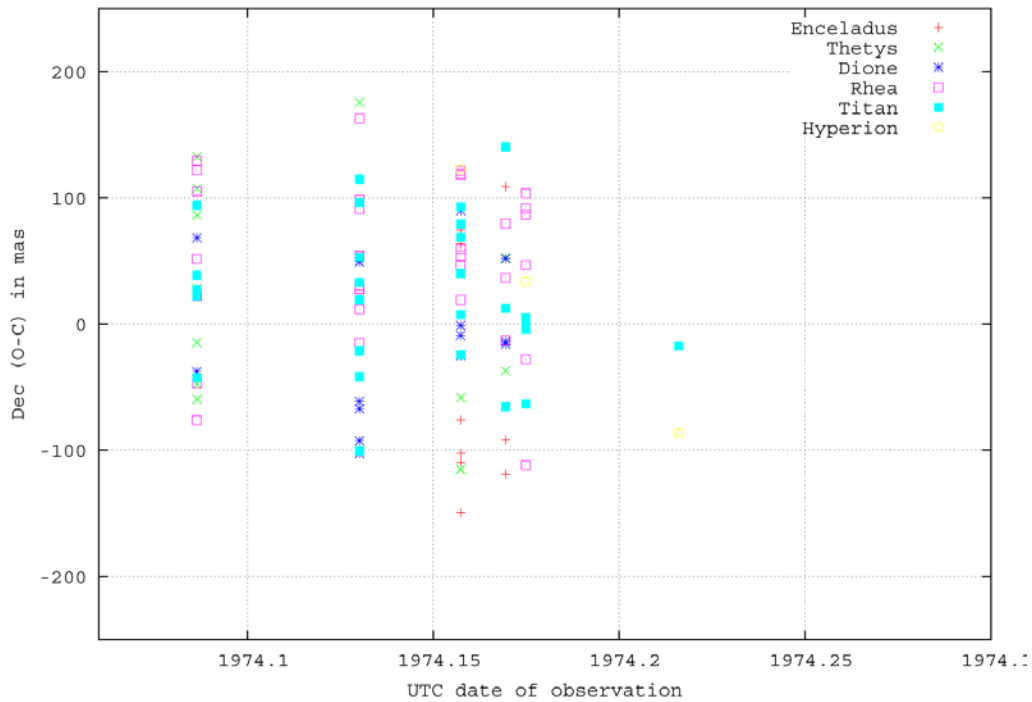
However, the first results are quite encouraging because the spherical (RA,Dec) accuracy, computed from about of 80 satellite positions, is about of 85 mas.

Because of the delay with the Martian new analysis, the IMCCE intends to come back to the Saturnian's in 2014 February. Because of the softwares are ever available and because the image analysis is not as complicated as the Martian's, it will be faster to analyze the complete collection. The IMCCE plans to provide the satellite positions and corresponding statistics at the end of April 2014.

2-III - Relevant images

The IMCCE analyzed parts of the DAMIAN images of the relevant photographic plates. This chapter summarizes which conditions were encountered and which methods were used to provide the results.

2-III.1 - DAMIAN images and preliminary treatment

From 2012 June to 2013 August, the IMCCE received 392 DAMIAN images of the South Africa Observatory Saturnian photographic plates from ROB.

III.1.1 - Negative to positive
Since the negative fits format is not convenient to extract all the available informations, the IMCCE converted the negative DAMIAN images provided by the ROB.

III.1.2 - Direct and reverse (D-R) digitization effect
The DAMIAN images were provided in direct and reverse modes by the ROB.

III.1.3 - Optical distortion

The DAMIAN optical distortion was corrected for each image by IMCCE with average data as mentioned in section I.1.4..

2-III.2 - Identification of the objects

A specific process was developed to extract, measure and identify the object positions on the images.

The stars and satellites were extracted and measured by means of the Source Extractor software. The objects were then identified by comparing with corresponding catalogs and ephemerides. The method was initially developed with the analysis of the USNO Galilean plates.

Because of the age of the plates, there are many damages visible on the images. Each observation should be analyzed manually and some of them could not be analyzed by the specific process. More, the star catalogs are inaccurate for these periods and number of references should be identified manually. This was the case for the following catalogs that were tested: Hipparcos, Tycho-2, UCAC2, NOMAD and UCAC3.

2-III.3 - Astrometric reduction

Because of the few available stars, the astrometric reduction is quite different with a common one.

III.3.1 - UCAC2 star spherical coordinates

The star catalog coordinates were directly corrected for all-known spherical effects such as the proper motions, the parallaxes, the light aberration, the relativistic light deflexion of the Sun and Saturn, and the total atmospheric refraction.

III.3.2 - UCAC2 star measured coordinates

The star measured coordinates could not be corrected for the instrumental coma-magnitude effect because no cluster plates could be used to estimate this contribution.

III.3.3 - Calibration of the field

When UCAC2 stars were available, the field was calibrated with a 6-parameters model, in order to provide (RA,Dec) positions.

III.3.4 - Measured positions

The measured satellite positions were corrected for the phase effect and for the above reverse effects to provide positions in a geocentric ICRS frame, outside the atmosphere. In consequence, no spherical corrections should be applied to use the data.

2-III.4 - Position results and discussion

The first results should be investigated in more details because the spherical (RA,Dec) accuracy can reach several arcseconds. In fact the residuals of the star reference reach the same order of magnitude and in a first approach, it is likely that observations taken before the 60's could not be reduced by using the available star catalogs for which the reference epoch is close to J2000. More, a problem of timescale could also introduce such errors but it should be confirmed.

Photographic plates of the natural planetary satellites were digitized by the Damian digitizer at ROB. From these plates, astrometric data were extracted and the list is presented in the table below; the list of the data provided in the NSDB data base are given at the end of the paper.

Table 2. Digitized plates data

Observatory	Objects	Images number	References
USNO Washington DC	Martian satellites	893 images	A&A 2015 vol.582,p.36
USNO Washington DC	Jovian satellites	1417 images	MNRAS 2011 vol.415, p.701
USNO Washington DC	Saturnian satellites	1289 images	A&A 2016 vol 506 p.37
USNO Flagstaff	Martian satellites	893 images	A&A 2014 vol.572,A104

3. Astrometric data from mutual events observations

3-I: What are the mutual events

The eclipses of the Galilean satellites by Jupiter were extensively observed during centuries, being the only source of astrometric positions of the satellites. Ephemerides were built thanks to these observations. Direct imaging replaces these observations as soon as it was possible to record the images and to measure them. However, the Galilean satellites are bright and difficult to measure referred to reference stars, fainter than the satellites. Looking for more accurate observations, we were able, after the 1970's to predict another type of event: the eclipses and occultations between the satellites themselves. The advantage is that the satellites have no atmosphere so that the shadow cones are very sharp and easy to model. During a mutual eclipse or occultation, the light received from the satellites decreases and increases for a few minutes. Contrarily to the eclipses by Jupiter, these events are very rare: they also occur near the equinox for the same reason than for the eclipses (when the Earth and the Sun are in the equatorial plane of the planet which is also the common orbital plane of the satellites) by the planet but the small size of the satellites makes the events to occur only during six months before and after the equinox. The figure below shows when the mutual events occur.
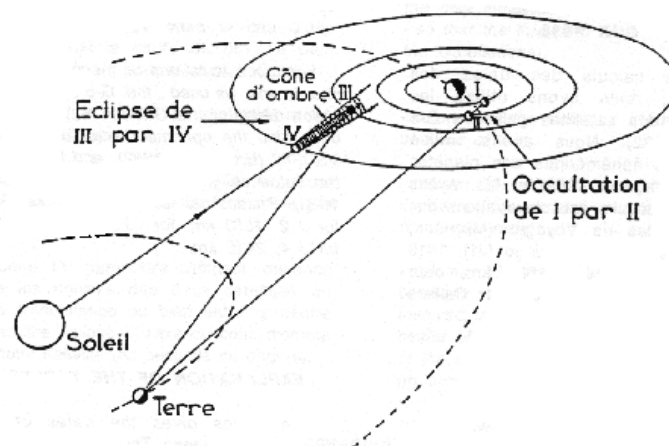

Figure the occurrence of mutual occultations and eclipses

The geometric configuration of the satellites during a mutual event allows getting their relative positions with an accuracy of a few kilometers. The eclipses by Jupiter provides the position of a satellite referred to the planet Jupiter and the mutual events position of a satellite referred to another satellite: this is not a problem since we know that the satellites are orbiting around the planet. Note that these events occur for the satellites of Jupiter, Saturn and Uranus.

The geometry of the observed mutual events

During an occultation, the disc of a satellite passes in front or behind the disc of another satellite. The light flux received from both satellite decreases compared to the flux of the satellites taken separately, have a minimum and come back to the value of the flux of the two satellites taken separately. A phenomenon occurs when the apparent distance between two satellites is smaller than the sum of the apparent radii (as seen from the Earth for the occultations and from the Sun for the eclipses). The phenomena may be partial, total or annular (as for the Moon). In the case of the eclipses, the eclipse may occur in the penumbra only, but this type of event may be more difficult to observe. We show on the figures below the aspects of the satellites during the events. For the occultations, we do not see such images from Earth since the telescope provides us only the diffraction figure. However, we are interested by the flux emitted by the satellites, not by their image. If the motion of the satellites was circular and without perturbations, the calculations for the predictions would be very simple: for each geocentric or heliocentric conjunction, a phenomenon would occur. It is not the case, and all the perturbating terms in the theory are to be taken into account. Thanks to electronic calculators, the calculations for the predictions may be completed without large errors. However, differences may appear between predictions and observations: the study of these differences may help for the improvement of the theory of the motions. Note that an eclipse is not an occultation seen from the Sun: it is an occultation of the Sun by the eclipsing satellite, as seen from the eclipsed satellite. The velocity of light may be carefully taken into account for the predictions and for the reduction.
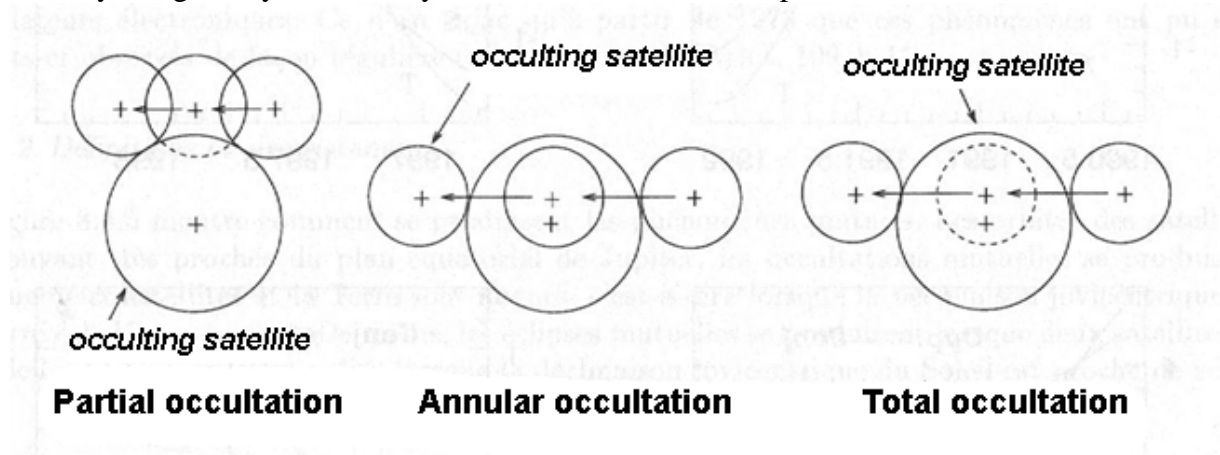
Figure: geometry of a mutual occultation

During an eclipse, a satellite enters the shadow of another satellite: the light flux will decrease, have a minimum and increase after the eclipse. The penumbra will make the light curve slightly different from the occultations. Note that for an occultation, the flux drop will depend on the relative brightness of the satellite. We have to know if the albedoes of the satellites are the same or not. This is not the case for an eclipse, independant of the albedoes.

24

eclipse: (a) by penumbra; (b) partial; (c) annular (total if $R_2 < R_u$)
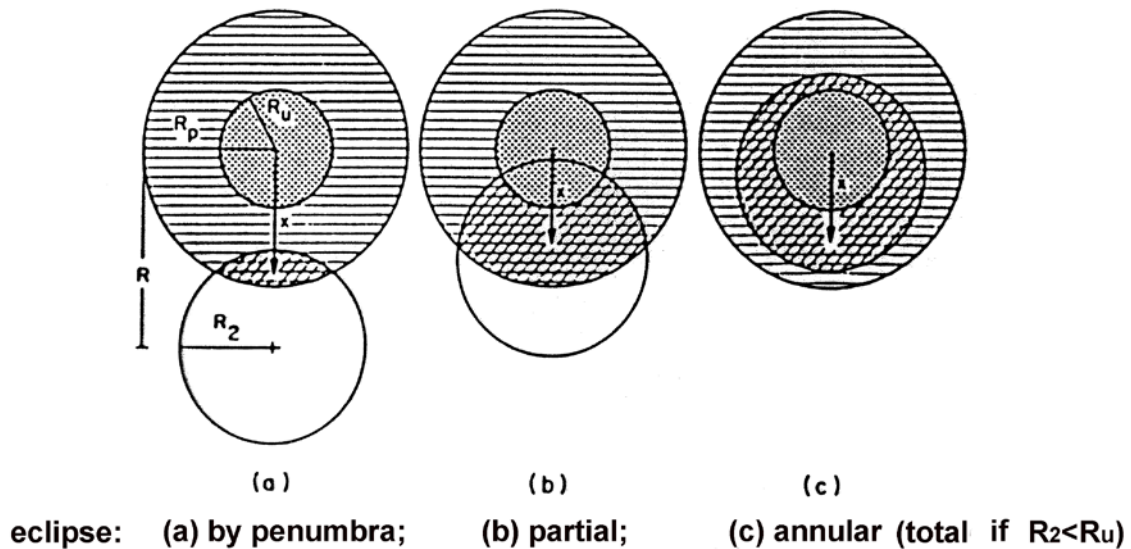
Figure: geometry of a mutual eclipse

What durations and magnitude drops during the mutual events?

The duration of the mutual events are most of time from 2 to 20 minutes of time. The grazing events may be very short with a small magnitude drop and difficult to catch. When one of the satellites is at its orbital elongation, a mutual event may be one hour or more long since the apparent velocities of the satellites are very small. The magnitude drop is small for grazing events and very large (100% decrease of the flux) for total eclipses. Note that during a total occultation, the occulting satellite is always visible and we have never a 100% flux drop. We will see below how is the light curve depending on the nature of the event.

When the mutual events occur ?

The events occur near the equinox on Jupiter during a few months due to the small size of the satellites and due to the small inclinations of their orbits on the equator of Jupiter. The figures below show the jovicentric declinations of the Earth and the Sun providing the periods of occurrence of mutual events. The last ones occurred in 2009 and 2015 for Jupiter and Saturn and in 2007 for Uranus. Note that the observability of the mutual events depends on other criteria: the occurrence of the opposition of the planet and the Sun which determines the period of observability of the planet and the declination of the planet which determines the zones of visibility on Earth (northern or southern hemisphere)

Figure the planetocentric declinations of the Sun and the Earth during the last occurrence of mutual events

Case of Jupiter-2009
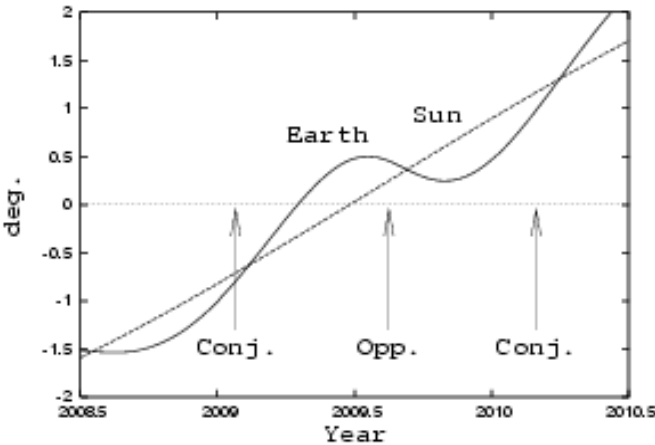
Case of Saturn - 2009
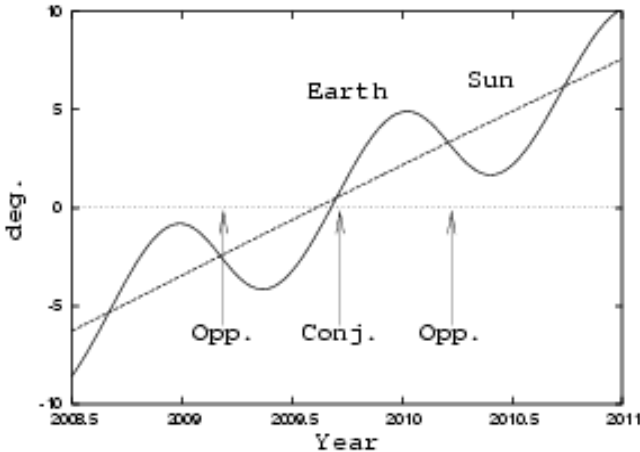
Case of Uranus in 2007
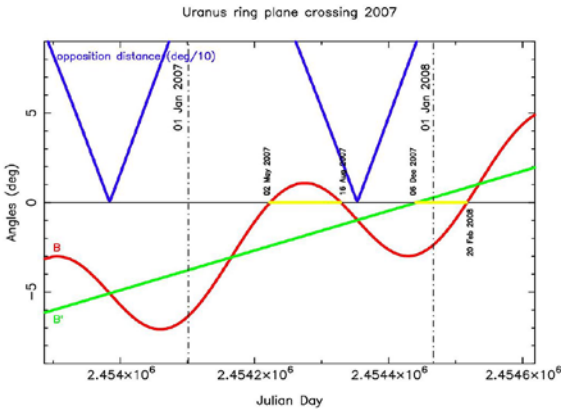
If the eclipses by the planets Saturn and Uranus are much more difficult to observe than the eclipses by Jupiter because of the too small apparent distance between the satellites and the planet at the time of an eclipse, the mutual events are more easily observable. However, the magnitude of the satellites is fainter and the apparent distances to the planets smaller than in the Jovian system that makes more difficult the observations. The principle of observation is the same for all the satellite systems but requires larger telescopes, more sensitive receptors and filters to decrease the brightness of the planet.

3-II: The observations

International campaigns of observations were made for the last occurrences in 2007 and 2009 for the Galilean, the Saturnian and the Uranian satellites. We used our network of observers as shown in the figure below:

Of course, all observing sites were not able to observe all events: it depends on the satellites to be observed as we will show it. More, during the observational campaigns, Jupiter and Uranus have a negative declination so that the sites in the southern hemisphere were more favourable for the observations.

The mutual events of the satellites of Jupiter

For the Galilean's small telescopes were used since the satellites are very bright. The system appears as shown by the image below. The observation of the satellites far from the planet Jupiter is easy. Amateur astronomers were asked for the observations and this explains the large number of observations made.

The Galilean satellites as seen in a small telescope

On such an image, the flux of the satellites involved in a mutual event will be measured in several windows as shown below in order to get the final flux drop which will be the data to be analysed for astrometric purpose.

When the sky background is uniform (that is the case, for example, if the satellites are far from the limb of Jupiter), the simplest is to simulate a photometer. It is enough so to calculate the sum of the pixels situated inside a window centered on a satellite (this window can be squared or circular). One will note S1 this sum and N1 the number of pixels. We will make the same calculation for a larger window around a smaller one. One will have then F1 and M1. We will calculate the sky background on the outer part of the second window (2). The light flux of the satellite is then calculated on the first window (3).

Calculation of the sky background: **Bg1 = (F1 - S1) / (M1 - N1)**   (2)

Light flux of the satellite: **Flux1 = (S1 / N1) - Bg1**   (3)

The only problem is to adjust the size of windows. It is not necessary to choose them too small because of the risk of losing a part of the object, nor too big what would add noise due to the too large part of sky. In practice it is necessary to make attempts, and to choose the combination which gives least variations onto the measures.
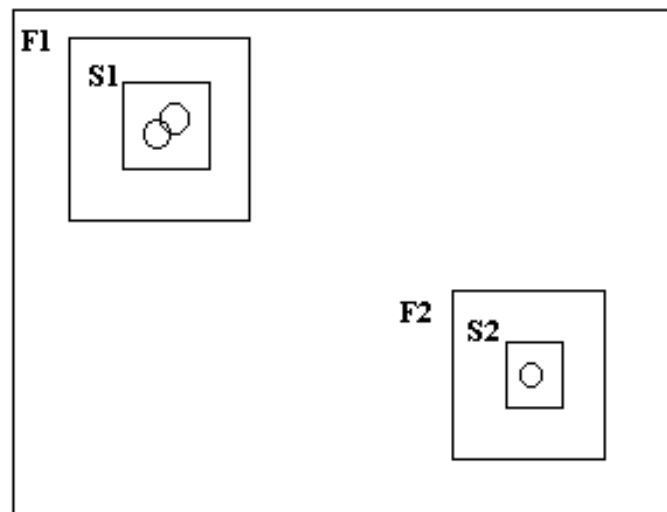
Another problem will come from light clouds not visible but decreasing the flux from the objects. This may make a false flux drop and must be avoided. If a reference object is present in the field (generally another Galilean satellites, rarely a bright solar-type reference), we may

calculate its light flux for each image. This flux is supposed to be a constant. If Flux2 is the light flux of the reference object S2 calculated as for Flux1, the light flux of the occulted or eclipsed satellite S1 will be:

Flux of satellite S1 = (Flux1 / Flux2) * FM2

where FM2 is the average flux of reference S2 , used in order to normalized the calculated flux of S1.
Then we obtain:

Flux of satellite S1 = ((S1/N1 - Bg1) / (S2/N2) - Bg2)) * FM2

This technique allows to observe events in difficult conditions: proximity of Jupiter (the background F1 and F2 may be very different), variation of the absorption or transit of light clouds (Flux1/Flux2 remains a constant), twilight (the sky background varies exponentially but is removed from each image). One will see the light curves corrected thanks to this method below in the next section "Reduction".

The mutual events of the satellites of Saturn

All this information may be applied to the satellites of Saturn. However, the observations are much more difficult since:
- the satellites are fainter (magnitude 8 to 14)
- the satellites seem to be closer to the planet since Saturn is at 10 astronomical units from the Sun and Jupiter at 5.
- the ring is very bright and the observations must be made far from the ring to avoid a light pollution of the photometric measure.

The image below shows the main satellites of Saturn in a mid-size telescope (1-meter).
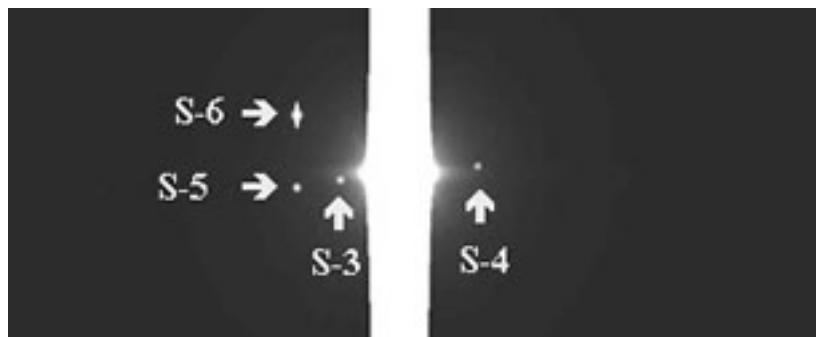
Figure: the system of the Saturnian satellites (field: 6 arcmin)

With such a field, the observations of mutual events should be made using a CCD receptor to get images that will be analyzed afterwards in order to extract the flux of the satellites. Note that for this system the use of a CH4 infra red filter may not be useful since it will darken the planet but not the rings which are very bright.

The mutual events of the satellites of Uranus

Same with the satellites of Uranus: same events, same techniques but with much more difficulties. Uranus is at 19 astronomical units from the Sun and the satellites seem to be very close to their bright planet. In this case, the use of a CH4 filter (2.2 micrometers) darkening the planet is very useful but the faintness of the satellites (magnitude 14 to 16) will make a large telescope necessary. The figure below shows the Uranian satellites as seen from different telescopes.

Figure: the satellites of Uranus observed in the V-band on a 1-meter telescope (field: 2 arcmin)
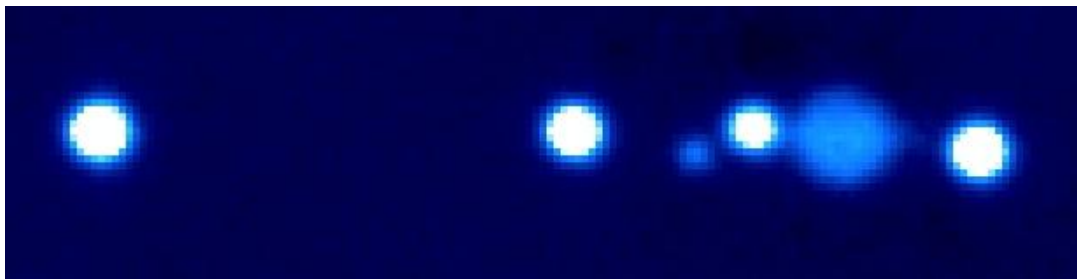
Figure: the satellites of Uranus observed with a CH4 filter on the NTT 3.5-meter ESO telescope (Uranus appears very dark at right)
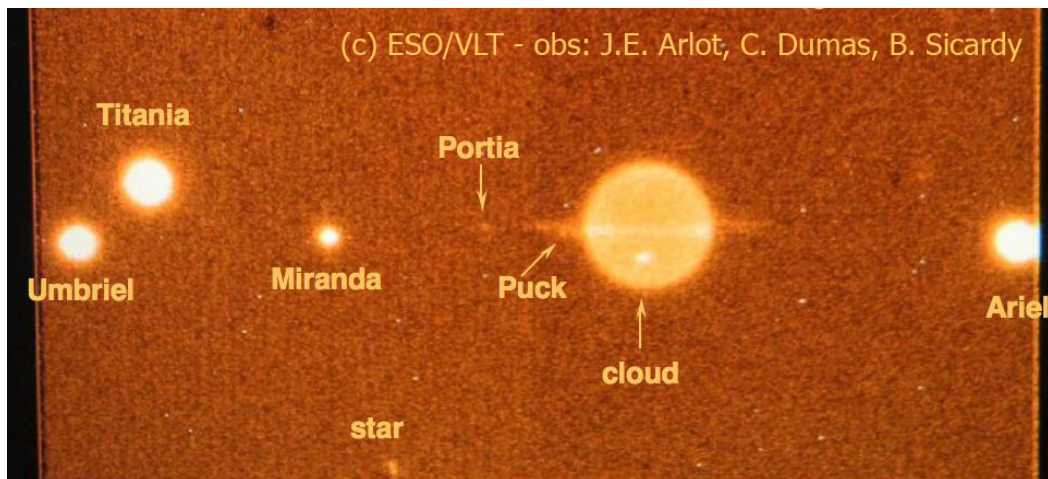
Figure: the satellites of Uranus observed with a CH4 filter and adaptive optics on the ESO-VLT 8-meter telescope.

The reduction of the observations

Receiving the raw data, we had to put them under a standard form in order to be able to extract astrometric information from the photometric observation. The light curves below are reduced light curves without instrumental or sky background effects. These light curves will be put in the database. Then, we will fit these light curves (inversion) with a model containing all the unknowns of the problem. Among these unknowns will be the astrometric relative positions of the satellites which will also put in the data base.

The examples of light curves below (from the Galilean satellites) show the different types of curves. Some are noisy, some are less noisy, some are symmetrical, some are not because of the phase effect which will be modelled as we will see it in the next section.
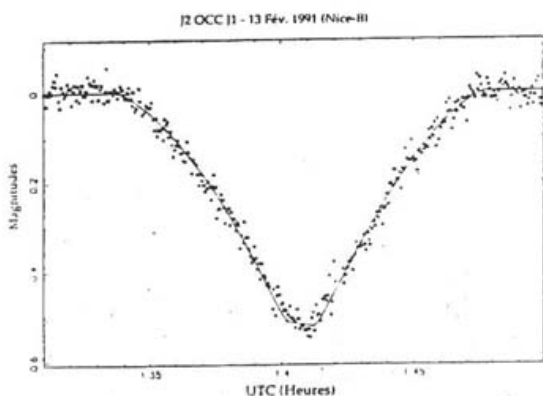
Symetrical deep lightcurve with the fit
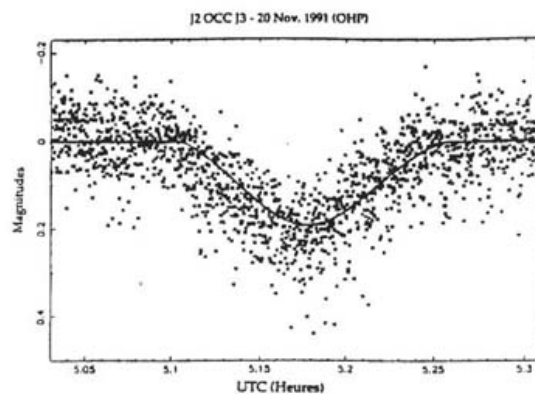
Other symetrical light curve with a worst signal/noise ratio and its fit
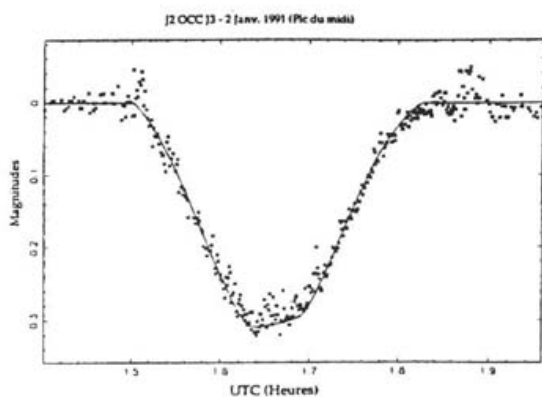
Non-symetrical lightcurve well fitted by the theoretical model.
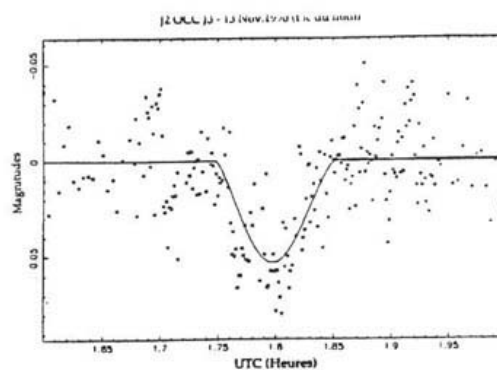
Grazing event with the fit based upon the theoretical model.

The figure below shows a light curve of an eclipse of the Uranian satellites (Titania by Umbriel taken at the VLT 8-meter telescope). The signal/noise ration is very good due to the size of the telescope and to the receptor used. In order to eliminate the light of the planet, we used an infra red camera in the K' band.
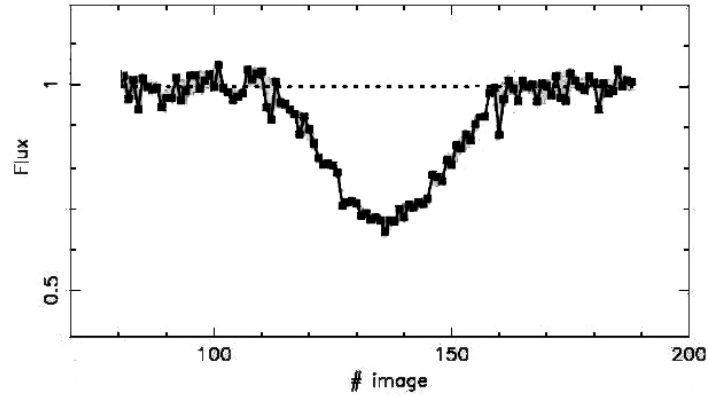
Figure: U-2 eclipses U-3, observed on the VLT

Extract astrometric information from the photometric observation.

Photometry of mutual occultation and eclipses of natural satellites allows accurate astrometric data to be obtained by reducing the derived light curves of the satellites. The flux coming into the receiver depends on the position of satellites. It depends as well on the reflective properties over the satellite surface, various laws of light scattering by a rough surface, wavelength-dependent solar limb-darkening, the wavelength-dependent sensitivity of the detector. To derive the satellite coordinates from the photometry results we inevitably have to model all other above-mentioned effects. The precision of the astrometric result depends therefore on the accuracy of this photometric model. Any simplification brings an error in the astrometric data. The influence of random errors in the photometry can be reduced using relevant statistical methods. These methods allow also to evaluate the astrometric accuracy of the observations. It will be denoted as "sigma". The errors caused by the inaccuracy of photometric model can not be reduced by statistical methods and can not be evaluated in any way. The "observation minus calculation" (O-C) residuals in the astrometric results contain all the errors including the errors delivered by the theory of satellite motion.

The summary of all performed international campaigns of observations can conclude about the astrometric accuracy of the mutual events observations. These estimates "sigma" comparing with observations of other kinds are shown in the following tables.

Kind of observation	Accuracy in mas	Accuracy in km
Eclipses by Jupiter	150	450
Old photographic plates	100	300
Transit circle	60	180
Plates newly reduced	50	150
CCD observations	40	120
Mutual events	15	45

Galilean satellites of Jupiter

Type of observation	Accuracy in mas	Accuracy in km
Automatic transit circle	30	200
Photographic plates	100	600
CCD observations	30	200
Mutual events	5	30

Main satellites of Saturn

Kind of observation	Accuracy in mas	Accuracy in km
CCD observations	40	400
Mutual events	6	60

Main satellites of Uranus

The figure below shows the residuals in arcsec of all the different kinds of observations. We may see that the mutual events observations have a similar accuracy than the HST observations.
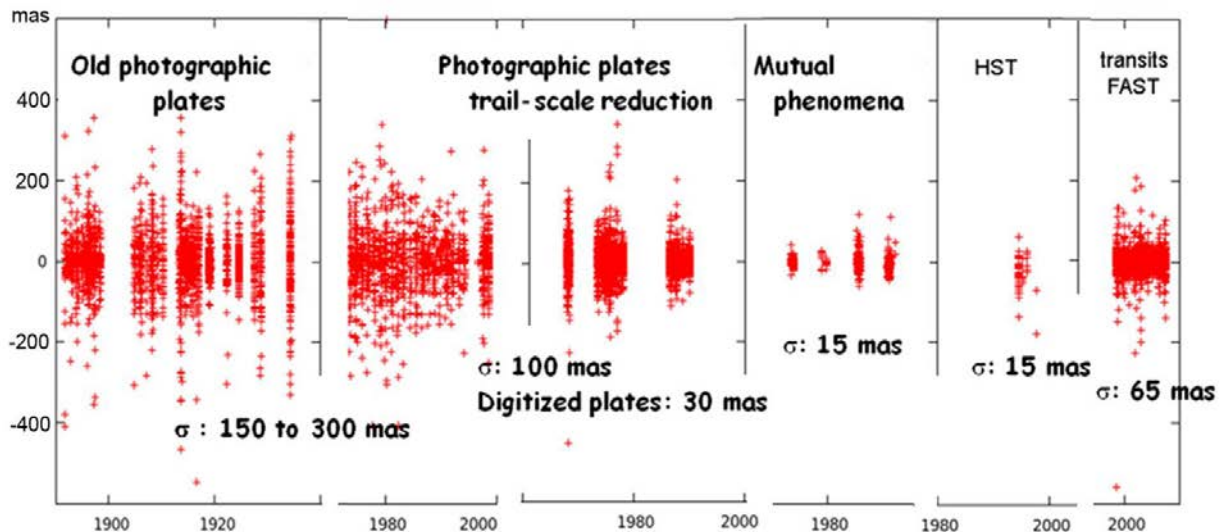
The inversion of the light curves

The inversion of the light curve is the modelling of the light curve and its fit to the observation in order to determinate the unknown parameters such as the astrometric relative positions of the satellites. Several models are available: we will use the one by Emelyanov (2003) and Emelyanov and Gilbert (2006).

The principal idea the method is to model the deviation of the observed relative satellite motion from the theoretical motion provided by the relevant ephemeris rather than analyze the apparent relative motion of one satellite with respect to the other.

a) the geometry of the events

Let X(t) and *Y(t)* are the projections of the differences of planetocentric Cartesian coordinates of the two satellites onto the plane of the event. In the case of mutual occultations, this plane coincides with the plane passing through the occulted satellite perpendicular to the line of sight of the observer. In the case of a mutual eclipse, the plane of the event passes through the eclipsed satellite perpendicular to the line connecting the satellite with the center of the Sun.

The coordinate origin is placed at the center of the *passive* (occulted or eclipsed) satellite. The occulting or eclipsing satellite is referred to as the *active* satellite. The following figures explain the geometric construction of the mutual events.
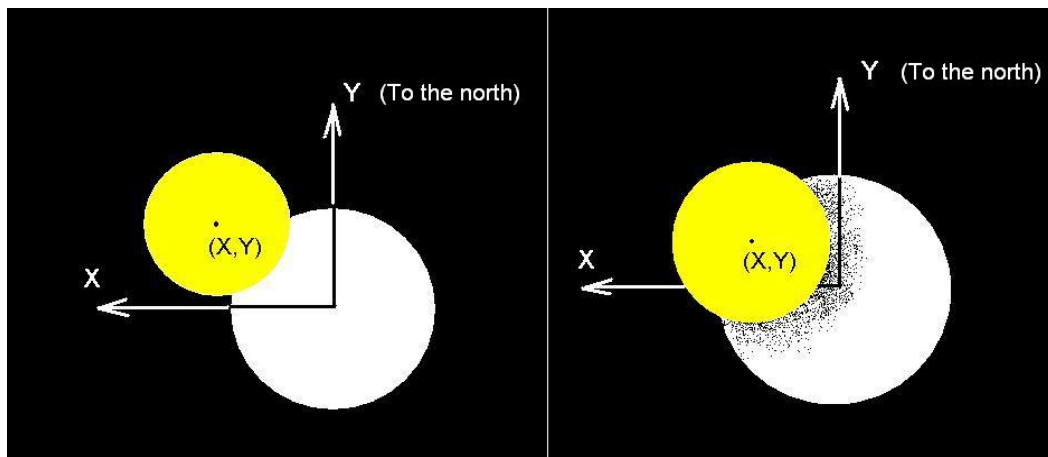
The left side shows the satellites during an mutual occultation as seen from the Earth. The mutual eclipse is an occultation of the Sun as seen from the eclipsed satellite and the astrometric data will be the apparent distance between the satellites as seen from the Sun (except that the light time are not calculated as when seen from Earth). It is shown in the right side of the figure where a penumbra is seen being larger than the eclipsing satellite. X and Y are the tangential coordinates of a satellite referred to the other. These are the astrometric data to be deduced from the photometric observation.

b) the flux

The measured flux E during an event at a given time t can be expressed by
$E(t) = K\, S(X(t), Y(t))$,
The function $S(X, Y)$ describes a model of the phenomenon. It is assumed that $S(X, Y) = 1$ outside each event. The unknown parameter K is a scale factor for the light drop during the event, equivalent to the total flux outside the event. The following figure shows changing of $S(X, Y)$ in time during the mutual event.
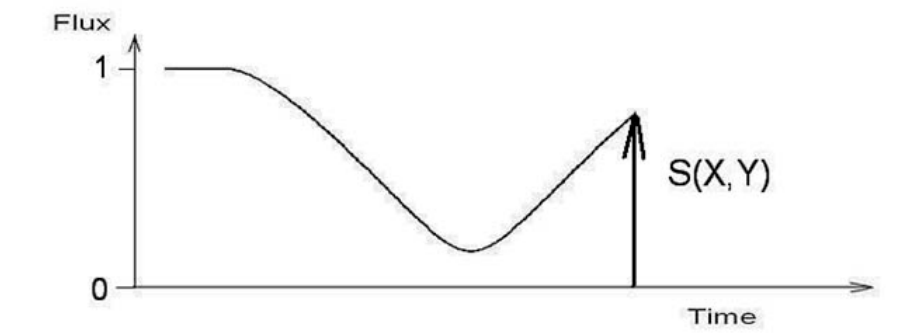
Given appropriate theories of the motion of planets and satellites, one can compute the theoretical values of functions $X(t)$, $Y(t)$, i.e., $X\mathrm{th}(t)$, $Y\mathrm{th}(t)$ for any time t. The real values of $X(t)$ and $Y(t)$ differ from $X\mathrm{th}(t)$ and $Y\mathrm{th}(t)$ by corrections Dx, Dy; i.e.,
$X(t) = X\mathrm{th}(t) + Dx$, $Y(t) = Y\mathrm{th}(t) + Dy$.

The assumption of the method is that corrections Dx and Dy remain constant during the observed event. According to our estimates, the error introduced by this assumption for Galilean satellites does not exceed 3.7 km in the satellite coordinates.

Our proposed method consists of solving conditional equations using the least-squares method
$Ei = K\ S(X\mathrm{th}(ti) + Dx, Y\mathrm{th}(ti) + Dy)$ $(i = 1, 2, ...,m)$
for constants Dx, Dy, K. Here Ei is the photometric count made at time ti. and m is the number of photomertric measurements during the observed event. We linearize conditional equations with respect to parameters Dx, Dy and then solve them using the least-square method. The result of reducing the photometric observations of a single event can be taken to consist of the following values:
$X(t^*) = X\mathrm{th}(t^*) + Dx,\ Y(t^*) = Y\mathrm{th}(t^*) + Dy,$
where t^* is an arbitrary time instant inside the event interval. We choose the time instant t^* as a time of the closest apparent approach of the satellites.

Any background flux registered in the receptor is supposed to be excluded. Our practice shows that some
unexpected parasitic background flux remains in the photometric measurements. A possibility is to add another constant P depending on the receptor and to have:
$Ei = K\ S(X\mathrm{th}(ti) + Dx, Y\mathrm{th}(ti) + Dy) + P$ $(i = 1, 2, ...,m)$

The conditional equations are to be solved in this case for constants Dx, Dy, K, and P. If we set $P = 0$ while incorrectly eliminating background so that this parameter actually differs from zero, an unaccounted systematic
error appears in parameter Dy.

The least-square method gives us also the error estimates $\Box_x$, $\Box_y$ of the values Dx, Dy. These are the errors caused by the random errors of the photometry. The values Dx, Dy themselves are differences between the astrometric results and a model of satellite motion adopted. They include the systematic errors due to the inaccuracy of photometric model taken into account.

c) building the model : the photometric function

The function $S\ (X,\ Y)$ describes a photometric model of the phenomenon. How to calculate this function?
Let's first build the photometric function of a **mutual occultation**

$F(\Lambda)d\Lambda$

dS_2

$f(\varphi, \lambda, i, e, \alpha, \Lambda)dS_2$

To the observatory :
$F(\Lambda)\ f(\varphi, \lambda, i, e, \alpha, \Lambda)\ d\Lambda\ dS_2$

$\Phi(\Lambda)$

From the receiver
$\Phi(\Lambda)\ F(\Lambda)\ f(\varphi, \lambda, i, e, \alpha, \Lambda)\ d\Lambda\ dS_2$

α - phase angle
i - incidence angle
e - reflectance angle
φ, λ - cartographic coordinates
Λ - wavelength

where :
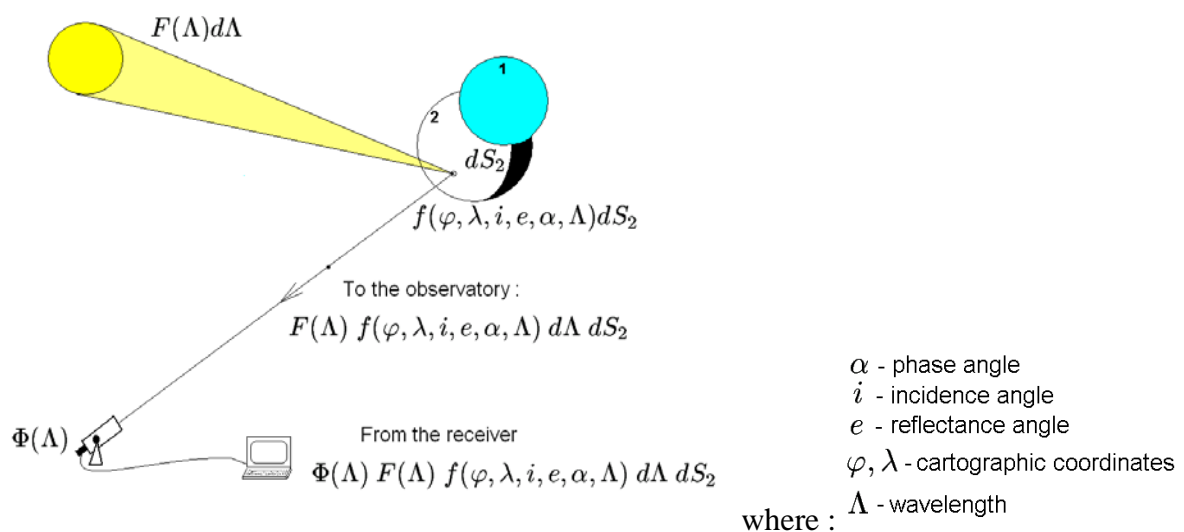
As we saw it previously, the flux S(X,Y) is supposed to be arrived on Earth and E (t) is the observed flux.

Let's build the function S:

Mutual occultation

$G_{\underline{b}}^{(p)}$ outside of the event $\Rightarrow$

$$S = \frac{G_b^{(a)} + G^{(p)}}{G_b^{(a)} + G_b^{(p)}} = \frac{1 + \frac{G^{(p)}}{G_b^{(a)}}}{1 + \frac{G_b^{(p)}}{G_b^{(a)}}}$$

$$G^{(p)} = \int\limits_{S_2} \int\limits_{\Lambda_1}^{\Lambda_2} \Phi(\Lambda)\, F(\Lambda)\, f_2(\varphi, \lambda, i, e, \alpha, \Lambda)\, d\Lambda\, dS_2$$

$$G^{(a)} = \int\limits_{S_1} \int\limits_{\Lambda_1}^{\Lambda_2} \Phi(\Lambda)\, F(\Lambda)\, f_1(\varphi, \lambda, i, e, \alpha, \Lambda)\, d\Lambda\, dS_1$$

In the case of mutual eclipse when the flux arriving from eclipsed satellite only the light passes as you see here:
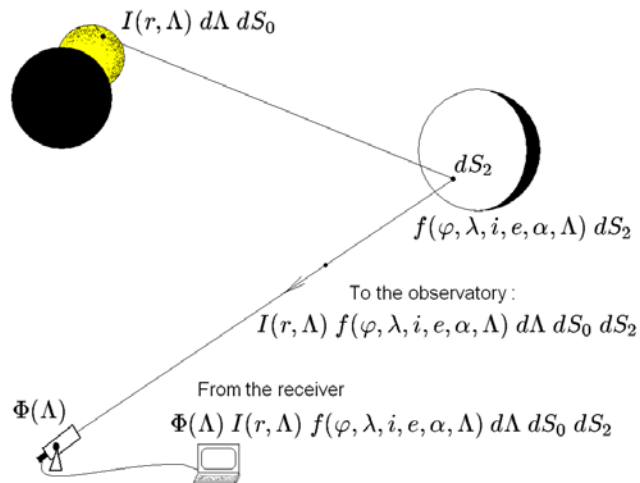
$I(r, \Lambda)\, d\Lambda\, dS_0$

dS_2

$f(\varphi, \lambda, i, e, \alpha, \Lambda)\, dS_2$

To the observatory :
$I(r, \Lambda)\, f(\varphi, \lambda, i, e, \alpha, \Lambda)\, d\Lambda\, dS_0\, dS_2$

From the receiver
$\Phi(\Lambda)\, I(r, \Lambda)\, f(\varphi, \lambda, i, e, \alpha, \Lambda)\, d\Lambda\, dS_0\, dS_2$

$\Phi(\Lambda)$

where :

α - phase angle
i - incidence angle
e - reflectance angle
φ, λ - cartographic coordinates
Λ - wavelength

In this case the function S can be build as follows:

Mutual eclipse

$$G^{(p)} = \int\limits_{S_2} \int\limits_{\Lambda_1}^{\Lambda_2} \Phi(\Lambda)\, f(\varphi, \lambda, i, e, \alpha, \Lambda) \int\limits_{S_0} I(r, \Lambda)\, dS_0\, d\Lambda\, dS_2$$

$$\boxed{G_b^{(p)} \quad \text{outside} \atop \text{of the event}} \longrightarrow \quad S = \frac{G^{(p)}}{G_b^{(p)}}$$
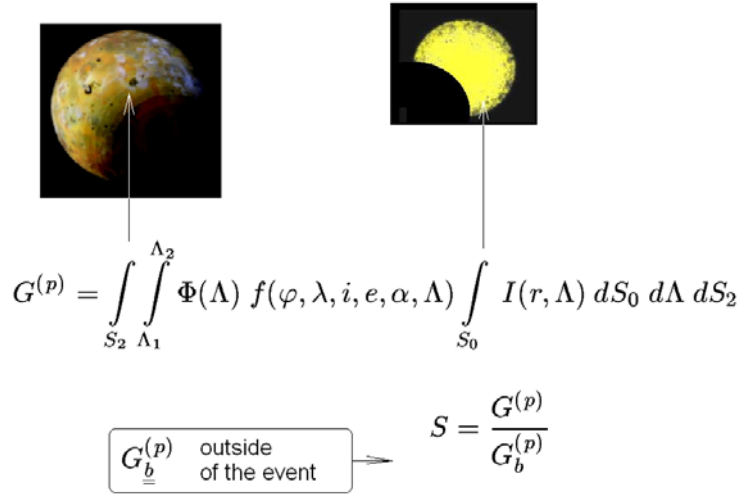
The function $f(\varphi, \lambda, i, e, \alpha, \Lambda)$ is the photometric function of a satellite. We have no source to determine this function. The following simplification can be applied

$f(\varphi, \lambda, i, e, \alpha, \Lambda) = R(i, e, \alpha, \Lambda)\, A(\varphi, \lambda, \Lambda),$

where $R(i, e, \alpha, \Lambda)$ is the pure photometric function deduced from the reflection-scattering laws and $A(\varphi, \lambda, \Lambda)$ is a function depending on the disk resolved albedo of the satellite i.e. on a map of albedo of the surface of the satellite. However, such maps are not always available. Then we replace the function $A(\varphi, \lambda, \Lambda)$ by a function $A(\theta, \Lambda)$ depending on the disk integrated albedo of satellite where θ is the angle of satellite rotation relative to the observer direction. The figure below shows how the function $A(\theta, \Lambda)$ is determined. Thus, we have $A(\theta, \Lambda) = P/P_0$ where P is the disk integrated albedo for given wavelength Λ and P_0 is the mean value of P. If there is no change of albedo A is equal to unit.

There can be various sources for searching the functions $R(i, e, \alpha, \Lambda)$ and $A(\theta, \Lambda)$. In fact, there are very few of them. We adopted the reflection-scattering law mounted by Hapke (1981, 1984) for the function $R(i, e, \alpha, \Lambda)$ with parameters taken from (McEwen et al. 1988, Domingue and Verbiscer 1997). We used the function $A(\theta, \Lambda)$ tabulated from observation by Morrison and Morrison (1977) and Prokof'eva-Mikhailovskaya et al. (2010) in V band of wavelength.

There we have shown that the reduced values of the astrometric result strongly depends on the adopted albedo ratio of two satellites involved in the mutual event.
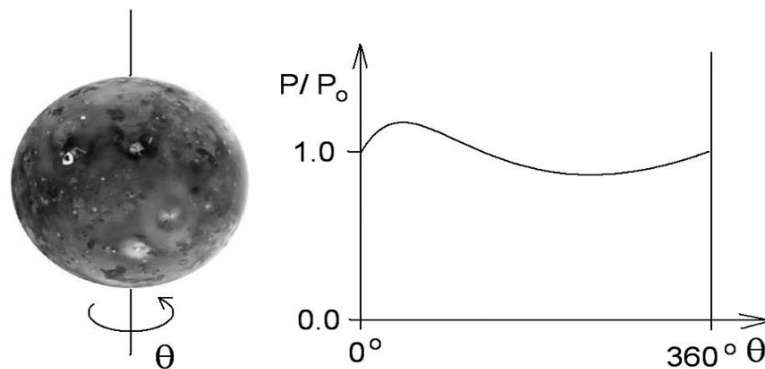
c) Analysis of the systematic errors

We have proved that there are two sources of significant systematic errors in the astrometric results obtained. They do not depend on a light scattering law applied. First source is a parasitic flux P incorrectly eliminated from the photometric measurements. Second is the inaccuracy of the satellite albedo adopted.

To increase the astrometric accuracy the methods of photometric processing of the observations must be revised and corrected to exclude parasitic flux P. A large photometric observations of Galilean satellites must be made to get correctly the function $A($ □□□□□ □□□

An attempt to repay these systematic errors was proposed in (Emel'yanov and Vashkov'yak, 2009). On the following figure the measured fluxes are shown: E_{12} - the combined flux from the occulted and occulting satellites together usually measured just before or after the phenomenon, E_1 and E_2 - the individual fluxes from the satellites measured before or after the event when they are sufficiently far from each other.
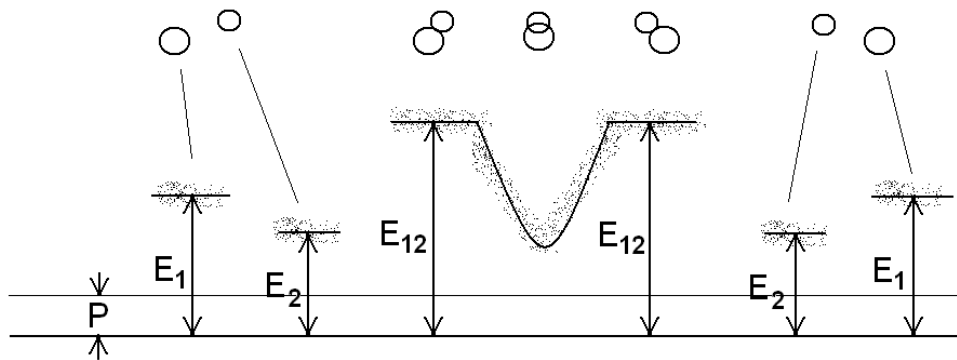
Let p_1 and p_2 are the albedo of the occulting and occulted satellites, respectively, and r_1 and r_2 are the radii of the apparent disks of the satellites. The relations

$$E_1 = Rp_1r_1^2 + P, \quad E_2 = Rp_2r_2^2 + P,$$

$$E_{12} = R(p_1r_1^2 + p_2r_2^2) + P,$$

$$P = E_1 + E_2 - E_{12}$$

$$\frac{p_2}{p_1} = \frac{r_1^2 E_{12} - E_1}{r_2^2 E_{12} - E_2}.$$

allow us to calculate the parasitic flus P and the ratio of the albedos p_2 / p_1. Here R is some undetermined coefficient. To apply this method it is necessary that R and P are staying constant during the period of observation of an event. In reality this is not always the case.

The results of the campaigns of observations

The table below provides the number of observations of the last campaigns of observations. Of course, due to the larger number of possible observational sites, the Galilean's were the most observed. Note that the final number of mutual event observations to be put in the data base will be smaller since we have to be sure to have all the metadata necessary for the reduction. All observations without all the needed information will be rejected.

	Number of light curves	Number of sites	Number of observed events	Number of observable events
Jupiter				
2009	520	52	240(*)	237
2015	609	75	236	442
Saturn				
2009	28	13	14	131
Uranus				
2007	36	16	27	193

(*): some events which were not selected as "observable event" (proximity of the Sun, proximity of the bright Jupiter) were successfully observed in spite of these unfavourable conditions.

The data

The data provided by the campaigns of observation of the mutual events are as follows:
-the light curves in a standard format in ascii files providing the dates of each photometric observation and the corresponding light flux observed. The sampling corresponds to the duration of the event. The first date (the starting point) is before the predicted beginning of the event and the last date is after the predicted end of the event. For each light curve, the metadata are provided in a ascii file (location of the observer, telescope used, filter, receptor, timescale,…).
-the astrometric relative positions of the satellites involved in each event. These data are extracted from the reduction of the light curves as explained above.

We do not provide the time of minimum of the light curve as we did for the first campaign since the information is included in the entire light curve.

The list of the data gathered and reduced are provided below.

Galilean satellites:

For the 2009 campaign, the tables below provide the observational site codes and the number of data for each site. The column labelled O gives the number of observations received from the observers, R the number of observations from which the astrometric results were obtained, N the number of observations where the light curves show no events, L the number of observations with incorrect data or missing metadata. The data were gathered, checked and analyzed in three places: A (IMCCE, Paris; B: Rio Observatory, Brazil and R: SAI, Moscow). The detector codes are provided in following tables.

Obs. code	O	R	N	L	Site, Country	Tel.	D cm	Det.	Longitude deg ′ ″	Latitude deg ′ ″	Alt. m
Source A:											
ASM:	1	1	0	0	Scaggsville, USA	SCT	20	CAM1	76 53 12 W	39 8 59 N	117
BBH:	1	1	0	0	Herne, Germany	T	20	CCD1	7 10 30 E	51 31 35 N	55
BCS:	7	7	0	0	Bucharest, Romania	SCT	30	CCD2	26 5 34 E	44 26 55 N	80
BCT:	3	3	0	0	Bucharest 2, Romania	T	15	CCD3	22 46 15 E	46 46 44 N	1400
BDX:	10	7	2	1	Bordeaux, France	T	62	CCD4	0 31 39 W	44 50 6 N	73
BLN:	24	24	0	0	Darfield, New Zealand	T	25	CAM2	172 6 24 E	43 28 53 S	200
BN:	1	1	0	0	Lille, France	L	32	CCD5	3 4 15 E	50 36 37 N	32
BTN:	9	9	0	0	Newark, USA	SCT	25	CAM3	77 7 7 W	43 0 24 N	165
CAL:	1	1	0	0	Anthon, France	T	23	CAM4	5 9 59 E	45 47 30 N	214
CED:	6	5	0	1	Edmond, USA	T	20	CAM5	97 31 3 W	35 39 44 N	339
CKE:	6	5	0	1	Kent, USA	T	25	CAM6	122 9 34 W	47 21 37 N	124
CM:	5	5	0	0	Armagh, Northern Ireland	T	15	CCD6	6 38 59 W	54 21 11 N	67
CPS:	3	3	0	0	Sabadell, Spain	MCT	13	CAM7	2 6 32 E	41 32 16 N	184
DC:	9	9	0	0	Kuriwa, Australia	T	25	CAM8	150 38 28 E	33 39 52 S	286
DH:	36	29	6	1	Kambah, Australia	SCT	35	CAM9	149 3 49 E	35 12 56 S	581
DO:	1	1	0	0	Sparta, Greece	SCT	25	CCD7	22 25 60 E	37 4 0 N	0
FA:	2	2	0	0	Keratea, Greece	SCT	23	CCD8	24 2 29 E	37 49 60 N	0
GA1:	19	19	0	0	Catania, Italy	T	20	CCD9	15 3 18 E	37 32 37 N	325
GA2:	2	2	0	0	Medelana, Italy	T	40	CCD10	11 9 9 E	44 21 44 N	651
GA3:	1	1	0	0	Gragnola, Italy	T	18	CCD11	10 6 31 E	44 11 21 N	0
GA4:	3	3	0	0	Catania M, Italy	T	20	CCD12	15 3 52 E	37 37 47 N	700
GA5:	4	4	0	0	Siena, Italy	L	10	CCD13	11 20 12 E	43 18 45 N	50
GA6:	1	1	0	0	La Spezia, Italy	L	20	CAM7	9 49 39 E	44 6 27 N	0
GA8:	9	9	0	0	Sorrento, Italy	T	25	CCD12	14 21 27 E	40 37 7 N	275
GA9:	3	3	0	0	Palermo, Italy	T	25	CAM10	13 20 20 E	38 9 14 N	30
GAC:	1	1	0	0	Ceccano, Italy	T	36	CCD14	13 19 43 E	41 34 6 N	190
GAN:	2	2	0	0	Catania N, Italy	T	20	CCD15	15 4 30 E	37 30 30 N	30
GAS:	2	1	1	0	GAS Pulkovo, Russia	T	50	CCD16	42 40 0 E	43 44 54 N	2070

Obs. code	O	R	N	L	Site, Country	Tel.	D cm	Det.	Longitude deg ′ ″	Latitude deg ′ ″	Alt. m
Source A (cont.):											
GB1:	14	14	0	0	Catania 23, Italy	T	23	CCD17	15 3 18 E	37 32 37 N	325
GB2:	1	1	0	0	Castel di Judica, Italy	T	11	CAM10	14 43 0 E	37 28 37 N	175
GB4:	12	12	0	0	Caselle, Italy	T	20	CCD18	9 47 52 E	45 5 54 N	44
GB6:	2	2	0	0	Ragusa, Italy	L	8	CCD19	14 43 60 E	36 55 0 N	40
GB7:	1	1	0	0	Castelnuovo, Italy	T	25	CAM11	10 0 28 E	44 6 17 N	325
GBC:	2	2	0	0	Castiglione, Italy	T	20	CCD12	15 3 51 E	37 48 55 N	1481
GD:	26	21	5	0	Nonndorf, Austria	T	25	CAM12	15 13 60 E	48 47 28 N	601
GJP:	10	9	0	1	Elgin, USA	T	20	CCD20	117 55 15 W	45 34 22 N	835
HP:	11	9	1	1	Marsfield, Australia	SCT	20	CAM13	151 6 12 E	33 46 14 S	89
JAN:	2	1	1	0	Akashina-Nanaki, Japan	SCT	25	CAM14	137 56 45 E	36 19 56 N	901
JGB:	2	2	0	0	Bartlesville, USA	SCT	20	CAM15	95 57 10 W	36 43 5 N	232
JGC:	1	1	0	0	Ochelata, USA	SCT	20	CAM15	95 59 51 W	36 35 60 N	262
JGO:	3	1	0	2	Sabadell 50, Spain	T	50	CCD21	2 5 29 E	41 33 4 N	224
JHS:	9	9	0	0	Okino, Japan	SCT	28	CAM16	136 12 25 E	35 6 6 N	140
JIM:	1	1	0	0	Mie, Japan	L	13	CAM16	136 33 34 E	35 7 10 N	92
JMS:	10	10	0	0	Moriyama, Japan	SCT	30	CAM14	135 56 34 E	35 6 22 N	85
JPP:	2	2	0	0	Sainte-Maxime, France	T	25	CAM17	6 35 60 E	43 45 4 N	30
JRM:	3	3	0	0	Moia, Spain	T	20	CCD22	2 5 44 E	41 49 5 N	822
JTN:	5	5	0	0	Waikanae, New Zealand	T	25	CAM30	175 1 57 E	40 51 20 S	5
JVM:	14	12	0	2	Mundolsheim, France	MCT	15	CCD24	7 42 46 E	48 38 48 N	140
KOU:	7	7	0	0	Kourovskaya, Russia	T	45	CCD35	59 32 50 E	57 2 12 N	280
LI:	5	5	0	0	Athens, Greece	SCT	40	CCD21-36	23 46 60 E	37 58 7 N	0
LNA:	1	0	0	1	LasNegras, Spain	T	20	CAM18	2 0 55 W	36 52 5 N	50
MD:	7	6	0	1	Tournefeuille, France	SCT	25	CAM17	1 19 34 E	43 34 59 N	158
MEU:	1	1	0	0	Meudon, France	T	100	CAM19	2 13 52 E	48 36 51 N	150
MUH:	1	1	0	0	Haast, New Zealand	T	15	CAM20	168 51 30 E	43 56 23 S	5
MU:	4	4	0	0	Christchurch, New Zealand	T	15	CAM20	172 38 27 E	43 29 49 S	10
OK:	4	4	0	0	Odessa, Ukraine	MCT	50	CAM21	30 45 20 E	46 28 40 N	86

Obs. code	O	R	N	L	Site, Country	Tel.	D cm	Det.	Longitude deg ' "	Latitude deg ' "	Alt. m
Source A (cont.):											
PAR	1	1	0	0	Parnon, Greece	SCT	25	CCD8	22 35 5 E	37 15 39 N	1420
PFC	4	3	0	1	Pic du Midi, France	SCT	20	CAM22	0 8 32 E	42 44 41 N	2860
RCS	2	1	0	1	Sabadell 16, Spain	L	16	CAM23	2 5 29 E	41 33 4 N	224
RVC	1	1	0	0	Chester, USA	SCT	35	CAM24	83 12 7 W	32 22 14 N	101
SB	3	1	0	2	Busto Arsizio, Italy	SCT	20	CAM25	8 51 9 E	45 36 11 N	235
SD	4	1	0	3	Columbia, USA	T	25	CAM26	86 59 43 W	35 31 36 N	231
SHS	1	1	0	0	Zhejiang, China	T	25	CCD25	119 36 15 E	30 8 0 N	993
TAA	6	6	0	0	Alma-Ata, Kazakhstan	T	60	CCD26	76 57 15 E	43 12 0 N	1450
TCK	1	1	0	0	Keratea M, Greece	MCT	12	CCD8	24 2 29 E	37 49 60 N	0
TC	3	3	0	0	Ellinogermaniki, Greece	SCT	40	CCD8-6	23 53 36 E	37 59 52 N	0
TG	11	4	0	7	Umatilla, USA	T	30	CAM19	119 17 46 W	45 55 20 N	98
TPB	6	2	4	0	Ukkel, Belgium	T	85	CCD27	4 21 28 E	50 47 51 N	105
TTS	1	1	0	0	Sounion, Greece	T	25	CCD8	24 1 0 E	37 40 0 N	0
TT	1	1	0	0	Lavrion, Greece	SCT	25	CCD8	24 2 60 E	37 43 0 N	0
VPP	4	4	0	0	Praha, Czech republic	T	30	CAM27	14 28 30 E	50 8 27 N	325
WEI	2	2	0	0	Weihai, China	T	100	CAM28	122 2 59 E	37 32 9 N	21
Source B:											
ITA	30	30	0	0	Itajuba, Brazil	T	60	CCD28	45 32 57 W	22 32 22 S	1860
Source R:											
CRI	15	15	0	0	Nauchny Z, Ukraine	T	60	CCD33	34 0 54 E	44 43 46 N	593
CRM	12	12	0	0	Nauchny RST, Ukraine	T	22	CCD34	34 0 54 E	44 43 46 N	593
GAS	20	20	0	0	GAS Pulkovo, Russia	T	50	CCD16	42 40 5 E	43 44 52 N	2070
P26	6	6	0	0	Pulkovo 26, Russia	T	60	CCD29	30 27 27 E	59 46 2 N	73
PNA	6	6	0	0	Pulkovo NA, Russia	T	33	CCD30	30 27 27 E	59 46 2 N	73
PUL	1	1	0	0	Pulkovo ZA, Russia	T	32	CCD31	30 27 27 E	59 46 2 N	73
TER	30	30	0	0	Terskol, Russia	T	60	CCD32	42 30 0 E	43 16 30 N	3100
VOR	3	3	0	0	Voronezh, Russia	T	50	CAM29	39 13 3 E	51 39 50 N	160
VO1	1	1	0	0	Voronezh 1, Russia	T	11	CAM29	39 28 39 E	51 53 59 N	100

Code used in the tables	Description
CCD1	Starlight SX with Sony ICX027BL chip
CCD2	field 10 × 7 arcmin
CCD3	field 6 × 4 arcmin
CCD4	CCD 2078 × 2048 pixels: field 10′ × 10′
CCD5	CCD Atik 16IC Sony ICX424AL 659 × 494 px
CCD6	SBIG ST-7XMEI
CCD7	SBIG ST-7
CCD8	Atik 16HR
CCD9	Meade DSI II Monochr.
CCD10	DMK 21 AU
CCD11	SBIG ST10-XME
CCD12	SBIG ST-7XME
CCD13	SBIG ST-7 ME
CCD14	SBIG ST-8XME cl1
CCD15	Meade DSI I Color
CCD16	CCD GAS-Pulkovo
CCD17	SBIG ST-7XME
CCD18	Meade DSI II Color
CCD19	Digital Reflex Canon Eos 400D
CCD20	SBIG ST402ME CCD Camera
CCD21	SBIG ST-8
CCD22	Mintron MTV-12V6EX
CCD24	SBIG ST9E
CCD25	CCD field 33 × 30 arcmin
CCD26	SBIG ST-7XE
CCD27	KODAK KAF-6300
CCD28	EEVCCD (cf. Dias et al. 2013)
CCD29	CCD FLI ProLine 09000
CCD30	CCD S2C
CCD31	SBIG ST-6
CCD32	PixelVision
CCD33	AP47p CCD
CCD34	PL16803
CCD35	Apogee Alta U6, Kodak KAF-1001E
CCD36	SBIG ST10-CCD

Code used in the tables	Description
CAM1	Mallincam Hyper Color Plus
CAM2	CCD Video PAL camera: 25 fps
CAM3	PC 164C video camera
CAM4	Watec 120N, Video Camera
CAM5	NTSC Video (PC164C w/ Iz filter)
CAM6	NTSC (PC164C unfiltered)
CAM7	Video CCD
CAM8	Video camera
CAM9	Watec 120-N+ video camera for recording
CAM10	CCD webcam Philips ToUCam Pro
CAM11	CCD webcam Philips
CAM12	Watec 120N, CCIR, 1/2" Sony CCD-Sensor ICX419ALL
CAM13	Watec 902H Video Camera
CAM14	SONY ICX428ALL
CAM15	Watec 902H2 Ultimate video camera
CAM16	SONY ICX429ALL
CAM17	Lumenera SKYnyx 2.0M
CAM18	CCD Video camera
CAM19	Watec 120N+ video camera
CAM20	CCD Video camera PAL 25 fps
CAM21	WAT-902H2 Sup
CAM22	Watec 120N. CCD Sony ICX-418ALL 1/2″
CAM23	Mintron (video camera) with Time Inserter KIWI
CAM24	Video camera on VHS tape digitized with a Dazzle DV 90 converter
CAM25	CCD webcam Philips Toucam Pro II
CAM26	GBC505E video camera
CAM27	Watec 120N, Video Camera
CAM28	no information
CAM29	Nikon D40 on June 16, otherwise Canon PowerShot A570 IS
CAM30	KPC-350BH video camera

For the 2015 campaign, the same data are provided in the table below. We provide the number of observations received O, the number of observations R for which astrometric results were calculated, the number of observations N for which the light curves showed no events, the number of observations S for which an occultation and an eclipse occurred at the same time and for which the astrometric results could not be obtained, the location of the observer, and if relevant their IAU code.

O	R	N	S	Site, Country	IAU code
11	10	1	0	Haute-Provence Obs., France	511
27	24	3	0	Pic du Midi Obs., France	586
48	47	1	0	Desert Springs, Australia	
3	3	0	0	Umatilla, USA	
41	41	0	0	Scottsdale, USA	
10	10	0	0	Kuriwa Obs., Australia	E28
9	7	0	2	Tunis, Tunisia	
16	15	0	1	La Couyere Astro. Center, France	J23
36	35	1	0	Murrumbateman, Austrialia	E07
14	14	0	0	Puig d'Agulles, Spain	
8	8	0	0	Tangra Obs., France	E24
5	5	0	0	Elgin, USA	440
5	5	0	0	Toulon, France	
10	10	0	0	Kourovskaya, Russia	168
8	8	0	0	Chaneyville, USA	
16	12	4	0	Mundolsheim, France	
5	5	0	0	Cogolin, France	
18	17	0	1	West Park Obs., England	Z92
5	5	0	0	Itajuba, Brazil	874
5	5	0	0	Iguacu, Brazil	X57
2	2	0	0	Como, Italy	C13
1	1	0	0	Arnold, USA	
3	3	0	0	Vesqueville, Belgique	231
11	11	0	0	Newark, USA	H95
2	1	1	0	Baronnies Provencales Obs., France	B10
7	7	0	0	Waikanae, New Zealand	
1	1	0	0	Kingman, USA	
5	4	1	0	Marseille, France	
6	6	0	0	Tielt, Belgium	
2	2	0	0	Dax Obs., France	958
2	2	0	0	Hyères, France	
3	3	0	0	Siena, Italy	K54
6	4	1	1	Trebur, Germany	239
1	1	0	0	Gardnerville, USA	
9	9	0	0	Montigny-le-Bretonneux, France	
2	2	0	0	Malemort-du-Comtat, France	
2	1	1	0	Darfield, New Zealand	
2	2	0	0	Gretz-Armainvilliers, France	A07
4	4	0	0	Cabudare, Venezuela	
2	2	0	0	Nikolaev, Ukraine	089
1	1	0	0	La Grimaudière, France	
6	3	3	0	Flynn, Australia	
7	7	0	0	Egeskov Obs., Danemark	
4	3	1	0	Salvia Obs., France	I73
11	11	0	0	Biesenthal, Germany	
2	2	0	0	Maidenhead, England	I64
6	6	0	0	Oberkrämer, Germany	
1	1	0	0	Wokuhl-Dabelow, Germany	
6	6	0	0	Rokycany Obs., Czech Republic	K61
6	6	0	0	Berlin, Germany	
1	1	0	0	Slovice, Czech Republic	
1	1	0	0	Fouras, France	
24	24	0	0	Vainu Bappu Obs., India	220
13	12	1	0	Horice, Czech Republic	
14	13	1	0	Alma-Ata, Kazakhstan	210

Saturnian satellites – Phemu09 campaign:

33 events have been observed and 26 fully reduced. The list follows:

UTC Date year m. day	Type of event	Site of observation		Filter	Sat. flux
2008 12 19	4o5	ATH	CCD3	Bessel I	4-5
	4o5	SAB	CCD1	Bessel R	4-5
	4o5	SAM	CCD8	Bessel R	4-5
	4o5	TER	CCD11	C	4-5
2008 12 22	2o3	SYD	CCD9	L	2-3
2008 12 24	3o2	ATH	CCD3	Bessell I	2-3
	3o2	MON	CCD6	L	2-3
	3o2	SAM	CCD8	L	2-3
	3o2	SCH	CCD8	L	2-3
	3o2	BOR	CCD12	C	2-3
	3o2	MEU	CCD2	L	2-3
2009 01 07	1o2	PIC	CCD0	L	1-2-3
2009 01 08	3o2	BOR	CCD12	C	3-2
	3o2	SCH	CCD8	L	3-2
	3o2	IT2	CCD14	I	3-2
2009 01 22	2e3	MTR	CCD5	R	1-2-3
2009 01 27	1o3	YUN	CCD12	R	1-3
2009 02 02	1e3	MTR	CCD5	R	1-3
	1e3	IT2	CCD14	I	1-3
	1e3	LAS	CCD15	Y	1-3
2009 02 04	1e3	GAS	CCD10	C	1-3
2009 02 06	2o3	MTR	CCD5	R	2-3
2009 03 23	1e2	LAS	CCD15	Y	1-3
2009 05 06	3e2	KAM	CCD2	C	2-3
2009 06 20	2e3	IT1	CCD13	methane	2-3
	2e3	IT2	CCD14	R	2-3
2009 07 01	4e5	DAR	CCD7	C	4-5
2009 07 02	3e4	UMA	CCD2	C	3-4-5
2009 07 07	3e4	ATH	CCD3	V	3-4
2009 07 14	4e5	IT1	CCD13	methane	1-3
2009 07 16	2e3	IT1	CCD13	methane	1-3
2009 07 19	4e1	LAS	CCD15	Y	1-3
2009 08 08	5e3	IT1	CCD13	methane	5-3

The meaning of the observing sites is as follows:

Sites	Code	Tel.	Rec.	Longitude ° ′ ″	Latitude ° ′ ″	Elevation m
Ellinogermaniki Agogi School Obs. (Greece)	ATH	T 40	CCD3	23 53 35 E	37 59 52 N	165
Canberra (Australia)	KAM	T 35	CCD2	149 03 48 E	35 23 49 S	582
Bordeaux (France)	BDX	T 60	CCD12	0 31 36 W	44 50 06 N	73
Darfield (New Zealand)	DAR	T 25	CCD7	172 06 24 E	43 28 53 S	210
Itajuba (Brazil)	IT1	T 160	CCD13	45 35 0 W	22 32 06 S	1870
Itajuba (Brazil)	IT2	T 60	CCD14	45 35 0 W	22 32 06 S	1870
CTIO, Cerro Tololo (Chile)	LAS	T 100	CCD15	70 48 53 W	30 09 55 S	2200
Meudon (France)	MEU	T 100	CCD2	2 13 54 E	48 48 18 N	162
Monterrey (Mexico)	MTR	T 35	CCD5	100 20 46 W	25 37 23 N	689
Montigny-le–Bretonneux (France)	MON	T 28	CCD6	2 00 52 E	48 45 54 N	168
Pic du Midi (France)	PIC	T 100	CCD0	0 08 34 E	42 56 11 N	2850
Pulkovo-Kislovodsk (Russia)	GAS	T 50	CCD10	42 40 04 E	43 44 52 N	2070
Sabadell (Spain)	SAB	T 50	CCD1	2 05 29 E	41 33 04 N	224
Sabadell (Spain)	SAM	T 50	CCD8	2 05 29 E	41 33 04 N	224
San Esteve Sesrovires (Spain)	SCH	T 40	CCD8	1 52 22 E	41 29 40 N	170
Sydney (Australia)	SYD	T 20	CCD9	150 38 34 E	33 39 37 S	271
Terskol (Russia)	TER	T 60	CCD11	42 30 03 E	43 16 36 N	3100
Umatilla (Oregon, USA)	UMA	T 30	CCD2	119 17 46 W	45 55 20 N	130
Yunnan Obs. (China)	YUN	T 60	CCD12	102 47 15 E	25 01 45 N	1940

The meaning of the receptors used is:

Code as given in the tables	Description
CCD0	camera Thomson THX 7863 384×288
CCD1	camera SBIG ST-8
CCD2	Video Watec 120N at 8 framestack
CCD3	Atik 16HR
CCD4	Video Watec 120N 25 frames/s
CCD5	SBIG STL1301-E
CCD6	SBIG ST8-XME
CCD7	TV camera PAL
CCD8	TV camera Mintron 12V6HC-EX
CCD9	TV camera Watec 120N at 16 framestack
CCD10	CCD SBIG STL-1001E
CCD11	CCD PixelVision Viena 1024×1024
CCD12	CCD DW436 2048×2048
CCD13	CCD S800 with methane filter
CCD14	CCD 301 with I filter
CCD15	Andicam with Y filter (IR)

Uranian satellites- Pheura07 camapign:

38 events have been observed and 36 fully reduced. They are listed below:

UTC Date year m. day	Type of event	Site of observation	Filter	Observed mid-time h m s	error in sec. +/-	Observed magnitude drop	error in mag. +/-	Sat.
2007 5 4	4o2	FAS	I'	19 9 56.13				4-2
2007 7 26	1e5	FAS	I'	19 12 56.93				1-5
2007 8 5	4o2	FAU	I'	13 53 48.81				4-2
2007 8 6	1o5	FAU	I'	10 35 30.86				1-5
2007 8 6	4o2	TNG	I	1 9 8.3	114.5	0.169	0.020	4-2
2007 8 13	1o2	ITA	I	3 6 6.0	8.0	0.362	0.019	1-2
2007 8 13	1o2	CLE	-	3 5 47.35				1-2
2007 8 13	1o2	NTT	K'	3 4 37.22				
2007 8 14	2o4	ATH	IR72	1 34 29.7	19.2	0.214	0.029	2-4
2007 8 14	2o4	ITA	I	1 33 59.2	7.5	0.211	0.016	2-4
2007 8 14	2o4	TUB	Ic	1 34 4.15				
2007 8 15	2o3	APO	I	9 16 40.1	3.8	0.561	0.016	2-3
2007 8 15	2o3	COV	R	9 16 50.9	15.5	0.484	0.108	2-3
2007 8 15	2o3	NTT	K'	9 15 50.17				2-3
2007 8 19	2o1	APO	I	7 59 51.1	9.7	0.412	0.016	2-1
2007 8 19	1o2	MON	R	7 59 55.6	30.6	0.444	0.069	1-2
2007 8 19	2o1	NTT	K'	8 0 15.10				2-1
2007 8 19	2o1	ITA	I	7 59 54.57				2-1
2007 8 22	2e5	FAU	I'	15 3 29.40				2-5
2007 8 24	1o2	FAU	I'	12 24 10.74				1-2
2007 10 8	1o5	ITA	I	0 43 40.8	19.2	0.312	0.167	1-5
2007 10 12	3e5	ITA	I	0 3 33.1	92.3	0.033	0.025	3-5
2007 10 12	4e5	FAU	I'	9 51 52.57				4-5
2007 11 28	1e3	ITA	I	1 41 46.81				1-3
2007 11 30	1e5	FAU	I'	8 53 57.09				1-5
2007 11 30	3e4	AGE	L	18 54 6.06				3-4
2007 11 30	3e4	AMP	Bessell R	18 48 39.97				3-4
2007 11 30	3e4	MAR	V	18 48 16.64				3-4
2007 11 30	3e4	SUT	Bessell I	18 48 43.37				3-4
2007 11 30	3e4	SAB	-	18 48 52.3	35.2	0.414	0.037	3-4
2007 12 4	2e1	APO	I	5 5 33.4	2.5	0.735	0.032	2-1
2007 12 7	1e2	APO	I	3 33 6.5	16.4	0.303	0.041	1-2
2007 12 7	1e2	MON	R	3 33 9.2	20.1	0.231	0.051	1-2
2007 12 8	2e3	MON	R	1 57 58.5	20.5	0.272	0.042	2-3
2007 12 8	2e3	VLT	K'	1 58 3.2	7.4	0.432	0.021	3
2007 12 15	1e3	HAN	Z	14 4 42.31				1-3
2007 12 17	4e3	HAN	Z	14 20 31.79				4-3
2008 1 4	1e5	TUB	Ic	16 16 54.73				1-5

The meaning of the codes of the observing sites and of the receptors is provided below:

Code as given in the tables	Description
CCD0	unknown
CCD1	camera SBIG ST-9XE
CCD2	Atik 16 Ic
CCD3	NACO (ESO Paranal UT4 telescope)
CCD4	Santa Barbara Instrument STL1301-E
CCD5	SITE ST-002 camera
CCD6	SBIG ST7-XME
CCD7	CCD Kodak Kaf 400L
CCD8	Agile High Speed photometer (APO telescope)
CCD9	Starlight SXV-H9
CCD10	CCD FLI-CM9
CCD11	wmv movie from video camera

Sites	Code	Tel.	Detectors	Longitude ° ′ ″	Latitude ° ′ ″	Elevation meters
Ager, Lleida (Spain)	AGE	T 25	CCD1	0 44 43 E	42 01 12 N	749
Ampolla, Tarragona (Spain)	AMP	T 36	CCD9	0 40 13 E	40 48 26 N	15
Apache Point, New Mexico (USA)	APO	T 250	CCD8	105 49 13 W	32 46 49 N	2788
Athens (Greece)	ATH	T 40	CCD17	23 53 36 E	37 59 52 N	0
Indian Hill Observatory, Huntsburg, Ohio (USA)	IHO	T 40	CCD6	81 04 52 W	41 32 48 N	389
Kent, Seattle, WA (USA)	COV	T 25	CCD11	122 9 34 W	47 21 36 N	124
Faulkes South, Siding Spring (Australia)	FAS	T 200	CCD16	149 3 42 E	31 16 24 S	1149
Faulkes North, Haleakala, Maui, Hawaii (USA)	FAU	T 200	CCD16	203 44 45 E	20 42 27 N	3055
Hanle (India)	HAN	T 200	CCD5	78 57 54 E	32 46 46 N	4500
Itajuba (Brazil)	ITA	T 160	CCD14	45 37 57 W	22 32 4 S	1864
Marseille (France)	MAR	T 20	CCD2	5 23 09 E	43 18 32 N	50
Monterrey (Mexico)	MON	T 35	CCD4	100 20 46 W	25 37 23 N	689
NTT, ESO-La Silla (Chile)	NTT	T 350	CCD18	70 43 54 W	29 15 40 S	2400
Pic du Midi (France)	PIC	T 100	CCD12	0 08 34 E	42 56 11 N	2850
Sabadell, Barcelona (Spain)	SAB	T 50	CCD10	2 05 29 E	41 33 04 N	224
SALT, Sutherland (South Africa)	SUT	T 1000	CCD15	20 48 38 E	32 22 33 S	1771
TNG, Canarian Islands (Spain)	TNG	T 360	CCD0	17 53 38 W	28 45 28 N	2387
TUBITAK, Antalya (Turkey)	TUG	T 150	CCD13	30 20 0 E	36 49 31 N	2539
VLT, ESO-Paranal (Chile)	VLT	T 800	CCD3	70 24 15 W	24 37 38 S	2635

The dissemination of the data

The data will be available under several forms. The first one will be publications in an international journal and the second one in the NSDB data base (Arlot et al. 2016). The first publication concerns the Saturnian satellites and the reference is give, below. The data have been included in the data base NSDB at the address nsdb.imcce.fr or directly at: ftp://ftp.imcce.fr/pub/databases/NSDC/saturn/raw_data/phenomena/mutual/2009/ which is accessible from the ESPaCE web site. All these data are also available directly from the NSDB data base at http://nsdb.imcce.fr.

Three campaigns of observation were reduced and astrometric data were calculated from these photometric observations. The detail of these campaigns is provided in the table below; the list of the data provided in the NSDB data base are given at the end of the paper.

Table 3. Mutual events data

Campaign	Objects	Observation number	References
Uranus 2007	Uranian satellites	34 light curves	Arlot et al. A&A 2013 vol.557, 4
Saturn 2009	Saturnian satellites	26 light curves	Arlot et al. A&A 2012 vol.544, 29
Jupiter 2009	Jovian satellites	457 light curves	Arlot et al. A&A 2014 vol.572,120
Jupiter 2014-15	Jovian satellites	609 light curves	Saquet et al. A&A 2017 in press
Jupiter 2014-15	Jovian inner satellites	4 light curves	Saquet et al. A&A 2016 vol 591 42

4. Astrometric data from relevant observations

Some CCD old and recent observations have never been reduced. In order to know the interest of this task, relevant observations were reduced as follows:

Table 4. CCD data

Observatory	Objects	Images number	References
Pic du Midi	Jovian inner satellites	54 images	Saquet et al. MNRAS 2017 vol 467, 694
USNO Flagstaff	Saturnian inner satellites	40 images	in preparation
ESO VLT	Uranian inner satellites	18 images	in preparation

Conclusion

In conclusion, 12 710 images or observations leading to more than 17 000 individual positions were selected and reduced in order to provide new astrometric observations allowing to improve the theoretical dynamical models and ephemerides of the natural planetary satellites. New ephemerides were made using these observations (Lainey 2016). All these observations are included in the database maintained by IMCCE and available on Internet through nsdb.imcce.fr or available via the ESPaCE ftp server as shown below.

The observational data are now also included in the NSDB data base (described in Arlot and Emelyanov, 2009) as follows. The relevant observations which were selected by data mining will be published in a future publication. Note that the CaViar software is available upon request.

Dissemination of the data in the NSDB data base:

Mars Express data:

Satellite	Dates	Number of observations	Series
Deimos	Aug. 1, 2005 to July 1, 2011	136	Pasewaldt
Phobos	May 17, 2004 to April 17, 2005	26	Obert
Deimos	Oct. 21, 2004 to Dec. 30, 2004	10	Obert
Phobos	Nov. 16, 2004 to Feb. 24, 2007	69	Willner

Cassini data:

Satellite	Dates	Number of observations
Mimas	June 22, 2004 to Feb. 4, 2011	876
Enceladus	June 21, 2004 to January 30, 2011	920
Tethys	June 20, 2004 to April 15, 2012	999
Dione	June 12, 2004 to Dec. 23, 2012	1361
Rhea	June 19, 2004 to April 20, 2012	1347
Iapetus	June 22, 2004 to June 10, 2011	1533

USNO Plates

Satellite	Dates	Number of observations	Telescope
Phobos	Aug.6, 1971 to March 20, 1997	424	26-inch
Phobos	April 17, 1967 to July 12, 1986	216	61-inch
Deimos	Aug.6, 1971 to March 20, 1997	450	26-inch
Deimos	April 16, 1967 to July 12, 1986	254	61-inch
Mars	Aug.6, 1971 to March 20, 1997	531	26-inch
Mars	April 16, 1967 to July 12, 1986	246	61-inch
Io	Nov. 19, 1967 to Nov. 4, 1998	1210	26-inch
Europa	Dec. 13, 1967 to Nov. 4, 1998	1248	26-inch
Ganymede	Nov. 19, 1967 to Nov. 4, 1998	1324	26-inch
Mimas	Feb. 17, 1974 to Dec. 16, 1997	123	26-inch
Enceladus	Nov. 13, 1973 to Dec. 16, 1997	275	26-inch
Dione	Nov. 13, 1973 to Dec. 17, 1997	509	26-inch
Rhea	Nov. 13, 1973 to Nov. 4, 1998	833	26-inch
Tethys	Nov. 13, 1973 to Nov. 4, 1998	376	26-inch
Titan	Nov. 13, 1973 to Nov. 4, 1998	950	26-inch
Hyperion	Feb. 27, 1974 to Oct. 6, 1996	27	26-inch
Iapetus	Nov.13, 1973 to Dec. 17, 1997	779	26-inch

Mutual events observations

Satellites	Dates	Number of observations
Jovian satellites	April 17 to Dec. 15, 2009	434
Saturnian satellites	Dec. 19, 2008 to July 16, 2009	26
Uranian satellites	May 4, 2007 to January 4, 2008	36

Relevant observations

Satellites	Dates	Number of observations
Amalthea	January to April 2015	35
Thebe	January to April 2015	19

Acknowledgements

Bibliographic references

Arlot, J.E., Saquet, E., Emelyanov, N.: 2015, The results of the 2015 campaign of observations of mutual events of the Jovian satellites, EPSC2015-50, communication to the European Planetary Science Congress, Sept. 27-Oct. 2, 2015, Nantes.

Arlot, J.-E.; Emelyanov, N.; Varfolomeev, M. I.; Amossé, A.; Arena, C.; Assafin, M.; Barbieri, L.; Bolzoni, S.; Bragas-Ribas, F.; Camargo, J. I. B.; and 84 coauthors: 2014, The PHEMU09 catalogue and astrometric results of the observations of the mutual occultations and eclipses of the Galilean satellites of Jupiter made in 2009, A&A 572, 120.

Arlot, J.-E.; Emelyanov, N. V.; Aslan, Z.; Assafin, M.; Bel, J.; Bhatt, B. C.; Braga-Ribas, F.; Camargo, J. I. B.; Casas, R.; Colas, F.; and 14 coauthors: 2013, Astrometric results of observations of mutual occultations and eclipses of the Uranian satellites in 2007, A&A 557, 4.

Arlot, J.E., N. V. Emelyanov, V. Lainey, M. Andreev, M. Assafin, F. Braga-Ribas, J. I. B. Camargo, R. Casas, A. Christou, F. Colas, D. N. Da Silva Neto, O. Dechambre, A. Dias-Oliveira, G. Dourneau, A. Farmakopoulos, D. Gaul9, T. George, D.L. Gorshanov, D. Herald, V. Kozlov, A. Kurenya, J. F. Le Campion, J. Lecacheux, B. Loader, A. Massallé, M. Mc Brien, A. Murphy, N. Parakhin, A. Roman-Lopes, C. Schnabel, A. Sergeev, V. Tsamis, P. Valdés Sada, R. Vieira-Martins, and X. Zhang : 2012, Astrometric results of observations of mutual occultations and eclipses of the Saturnian satellites in 2009, A&A 544, A29

Arlot, J.E., Emelyanov, N.: 2009, The NSDB Natural Satellite Data base, Astronomy and Astrophysics, Volume 503, Issue 2, 2009, pp.631-638

Cooper, N. J.; Murray, C. D.; Lainey, V.; Tajeddine, R.; Evans, M. W.; Williams, G. A: 2014, Cassini ISS mutual event astrometry of the mid-sized Saturnian satellites 2005-2012, Astronomy & Astrophysics, Volume 572, id.A43, 8

Domingue, D., & Verbiscer, A. 1997, Icarus, 128, 49

Duxbury, T.C., Callahan, J.D., 1988. PHOBOS and Deimos astrometric observations from Viking. Astron. Astrophys. 201, 169–176.

Emelyanov N. V., Gilbert R.: 2006, Astrometric results of observations of mutual occultations and eclipses of the Galilean satellites of Jupiter in 2003, Astronomy and Astrophysics. V. 453. P. 1141-1149.

Emelianov N.V.: 2003, A Method for Reducing Photometric Observations of Mutual Occultations and Eclipses of Planetary Satellites, Solar System Research. 2003. Vol. 37. No.4. P. 314-325.

Emel'yanov N. V., Vashkov'yak S. N. (2009) Mutual Occultations and Eclipses of the Galilean Satellites of Jupiter in 1997: Astrometric Results of Observations Solar System Research. 2009. V. 43. No. 3. P. 240-252.

Hapke, B. 1981, J. Geophys. Res., 86, 3039

Hapke, B. 1984, Icarus, 59, 41

Lainey, V.: 2016: Ephemerides of the Natural planetary satellites of Mars, Saturn and Uranus provided by the FP7 program ESPaCE, Note scientifique et technique de l'IMCCE NST 106, IMC Editions, Paris 2016, ISSN 1621-3823, ISBN 2-910015-77-7

McEwen, A. S., Johnson, T. V., & Matson, D. L. 1988, Icarus, 75, 450

Morrison, D., & Morrison, N. D. 1977, in Planetary satellites (Tucson:University of Arizona Press), 363

Oberst, J., Schwarz, G., Behnke, T., Hoffmann, H., Matz, K.D., Flohrer, J., Hirsch, H., Roatsch, T., Scholten, F., Hauber, E., Brinkmann, B., Jaumann, R., Williams, D., Kirk, R., Duxbury, T., Leu, C., Neukum, G., 2008. The imaging performance of the SRC on Mars Express. Planet. Space Sci. 56, 473–491. doi:10.1016/j.pss.2007.09.009

Pasewaldt, A., Oberst, J., Willner, K., Wählisch, M., Hoffmann, H., Matz, K.-D., Roatsch, T., Hussmann, H., Lupovka, V., 2012. New astrometric observations of Deimos with the SRC on Mars Express. Astron. Astrophys. 545, A144. Doi:10.1051/0004-6361/201118603

Prokof'eva-Mikhailovskaya, V. V., Abramenko, A. N., Baida, G. V., et al. 2010, Bull. Crimean Astrophys. Obs., 106, 68

Saquet, E.; Emelyanov, N.; Colas, F.; Arlot, J.-E.; Robert, V.; Christophe, B.; Dechambre, O.: 2016 Eclipses of the inner satellites of Jupiter observed in 2015 Astron. Astrophys 591 42

Saquet; E, N. Emelyanov, V. Robert, J.-E. Arlot, P. Anbazhagan, J. Bardecker, A.A. Berezhnoy, M. and 107 co-authors: 2017, The PHEMU15 catalog and astrometric results of the Jupiter's Galilean satellite mutual occultation and eclipse observations made in 2014-2015 Astron. Astrophys. In press

Tajeddine, R.; Cooper, N. J.; Lainey, V.; Charnoz, S.; Murray, C. D.: 2013, Astrometric reduction of Cassini ISS images of the Saturnian satellites Mimas and Enceladus, Astronomy & Astrophysics, Volume 551, id.A129, 11

Willner, K., Oberst, J., Wählisch, M., Matz, K.D., Hoffmann, H., Roatsch, T., Jaumann, R., Mertens, V., 2008. New astrometric observations of Phobos with the SRC on Mars Express. Astron. Astrophys. 488, 361–364. doi:10.1051/0004-6361:200809787